THEORETICAL NUCLEAR PHYSICS

Nuclear Reactions

HERMAN FESHBACH
Massachusetts Institute of Technology
Cambridge, Massachusetts

A Wiley-Interscience Publication
JOHN WILEY & SONS, INC.
New York / Chichester / Brisbane / Toronto / Singapore

Library of Congress Cataloging in Publication Data:

Feshbach, Herman.

Theoretical nuclear physics : nuclear reactions / Herman Feshbach.

p. cm.

"A Wiley-Interscience publication."

Includes bibliographical references and index.

ISBN 0-471-05750-9

1. Nuclear reactions. 2. Scattering (Physics) I. Title.

QC794.F43 1991 91-4668

539.7'5—dc20 CIP

Printed in the United States of America

10 9 8 7 6 5 4 3 2 1

Printed and bound by Courier Companies, Inc.

To Amos de Shalit, Friend and Colleague

CONTENTS

PREFACE

The development of the experimental and theoretical understanding of nuclear reactions is one of the more important achievements in physics during the last half of this century. It is an achievement which has been largely unrecognized or celebrated, even by the nuclear physicists themselves. It was accomplished without detailed knowledge of the underlying governing nuclear forces. Nevertheless, through ingenious use of physical principles and analogies and through the synergism of experiment and theory, a coherent and powerful methodology has evolved, one capable of interpreting the wide range of experimental nuclear studies and providing at the same time insights into the nature of the nuclear Hamiltonian. We have learned to distinguish and treat various types of reactions. We have learned how a reaction proceeds, which reactions and projectiles are most suitable for probing the structure of the nucleus, how the various degrees of freedom of nuclear systems such as the giant resonances manifest themselves in reactions, what the influence the Pauli principle is, when statistical methods are applicable touching in this way on nonequilibrium statistical mechanics, and so on. The power of these procedures is revealed when new areas of interest come under study, for one finds that one can apply them, adjusted for the new circumstances and in a suitable range of kinematic parameters, to obtain a quantitative understanding. This is not meant to imply that the theory is complete. As nuclear physicists become involved with quark-gluon degrees of freedom, new procedures, which may or may not be generalizations, may be required. The incorporation of relativity and of quantum fields form major challenges. But we do have a firm, well-understood base from which to begin.

These results are not of value only for nuclear collisions. They are valid and

have been applied to collisions between atoms, between molecules, and to collisions of these systems with electrons and photons. Some have recently become of interest to students of mesoscopic systems. It is this universal applicability which gives nuclear reactions its seminal importance.

Following the introductory Chapter I, Chapters II and III (Multiple Scattering and the Formal Theory of Nuclear Reactions) set the stage for the applications which follow. These two chapters provide the theoretical foundation which in the subsequent chapters is generalized and approximated as needed. Chapter IV (Compound Nuclear Resonances) deals with reactions involving long interaction times, while Chapter V and Chapter VI consider the limiting short interaction time reactions as seen in elastic and inelastic scattering and in particle and cluster transfer. In Chapter IV statistical approximations are introduced, while in Chapter V and Chapter VI the optical model and single-step direct reactions play dominant roles. Reactions involving interaction times which are intermediate, neither so long as those which prevail in the resonance region nor so short as implied by the single-step direct interactions, are considered in Chapter VII. This chapter is concerned with coupled equations and the statistical multistep compound and direct theories, which can be thought of as an approximate way of solving systems of many coupled equations. Chapters II through VII provide a formalism, together with examples, which enables one in principle to deal with most nonrelativistic reactions. This account of course reflects my own personal point of view and experience.

Chapters VIII through X differ in character from the earlier chapters in that they deal with subjects rather than with reaction types. Examples of the use of the analysis of the preceding chapters and generalizations thereof, as well as in some cases special methods which have been proved to be of value, are described. Chapter VIII considers heavy-ion reactions, Chapter IX reactions with high energy projectiles including electrons, nucleons, and heavy ions briefly, and Chapter X the interaction of pions and kaons with nuclei.

It is not possible to be complete or up to date. After all, the *Treatise on Heavy Ion Science*, edited by D. A. Bromley, consists of four large volumes and even it is not complete. A selection had to be made. In each case I try to present an overview of the subject together with a number of topics which I think are important and which in addition illustrate concepts and methods described in the earlier chapters. It is my hope that this will make the current literature and review articles accessible to the reader.

I have assumed a good understanding of nonrelativistic quantum mechanics, especially of scattering theory. A summary of that theory is presented in an appendix. The appendix also contains a general formalism for polarization phenomena. In the main body of the book only the polarization variables which occur in the scattering of spin-1/2 particles by spin-zero systems are discussed in detail.

The reader will find many references to the book with de Shalit entitled *Theoretical Nuclear Physics: Nuclear Structure*. That book has been reissued (with some major errors removed) in a paperback edition in the Wiley Classics Library (1990).

No attempt has been made to determine priorities. In view of the enormous relevant literature this just by itself would be a major project. The bibliography contains references to publications which I found useful and to papers referred to in the text. At the beginning of most sections I have listed the principal references I have consulted and/or review papers which provide a more detailed discussion of the subject of the section.

A number of people have been of great help to me. I particularly want to thank Viki Weisskopf, a dear friend and teacher, for his inspiring example and for the many years we have spent together discussing physics and plotting to do our share in improving the human condition: Peace rather than war, mutual respect rather than bigoted hostility. I own much to Arthur Kerman with whom I collaborated on several papers on nuclear reactions. I want to thank my friends who took time out from their busy lives to read and comment on most of this volume: A. Gal, read Chapters I to IV; M. Baranger, Chapter IV; Norman Austern, Chapters VI to VIII; A. Molinari, Chapter IX; and F. Lenz, Chapter X. T. Matsui read the sections in Chapter IX on high energy heavy-ion reactions. I am grateful to E. Moniz for supplying me with a preliminary version of his review article on pion physics with F. Lenz, to L. Ray for his advice on the proton–nucleus discussion in Chapter IX, and to J. Negele for several helpful suggestions. The supportive atmosphere of the MIT Center for Theoretical Physics, the friendship I have enjoyed with its faculty for many years, and the wide range of available expertise within the group and in the MIT Department have been of inestimable value as I pursued the writing of this book for more than a decade while undertaking and carrying out many other responsibilities. Roger Gilson helped to prepare most of the manuscript for publication. I am indebted to him for his thoughtful and expert assistance.

Most importantly I want to thank my wife, Sylvia, who for more than fifty years has been my companion and friend. Her understanding and encouragement were essential ingredients in executing and completing this project.

THEORETICAL NUCLEAR PHYSICS

CHAPTER I

INTRODUCTORY REVIEW

1. INTRODUCTION

Nuclear reactions present an extraordinarily rich and diverse set of phenomena. They are the principal source of information regarding nuclear systems. Their discovery and investigation are made possible because of the large number of projectiles available, each of which can interact with nearly all the stable nuclei, because of the precision with which the energy and general quality of the projectile beams can be controlled, because of the sensitivity of the detectors, and because of the theoretical framework available for the analysis of the data obtained.

A list of elementary particles most of which can and have served as projectiles is given in Table I.10.1 in deShalit and Feshbach (74). The strongly interacting projectiles of interest include the elementary bosons, such as the pion and kaon; the elementary baryons, such as the nucleons; the antiprotons and strange baryons; and an expanding number of the atomic nuclei, ranging from the deuteron to uranium. Clearly, these projectiles provide a wide range in mass, charge, isospin, strangeness and internal structure. Electromagnetic probes include γ-rays and charged particles such as the electron, the muon, the α-particle, and heavy ions—to mention those that have been used for this purpose. Reactions in which electron or muon neutrinos (or antineutrinos) are projectiles or are produced are used to study the effects of the weak interactions. These interactions are also responsible for symmetry violations, which are investigated by means of reactions sensitive to parity conservation or time-reversal invariance.

In most cases the projectiles are stable or have a relatively long life. The question arises: Can the interactions of very unstable particles whose lifetimes

are very short, such as the $\pi^0 (\tau \sim 0.83 \times 10^{-16}\,\text{s})$, the $\rho (\tau \sim 4.3 \times 10^{-24}\,\text{s})$, or the $\Delta (\tau \sim 5.7 \times 10^{-24}\,\text{s})$, be studied? The distances these particles travel before decay is far too small for it to be possible to prepare a beam. The distance between the source and the target is, under ordinary circumstances, far too large. However, this distance can be reduced if the source is inside the target for π^0 or inside a nucleus for the ρ meson or the Δ. In the first case, the π^0 can travel a distance on the order of the interatomic distances in matter before decaying. In the second, the ρ (or Δ) produced by the interaction of an energetic particle with a nucleon inside a target nucleus will live long enough to interact with a neighboring nucleon and thus permit a measure of the ρ-nucleon cross section.

An important measure of the quality of an experimental arrangement is the energy resolution that can be obtained. The first excited state of nuclei varies in energy above the ground state from a few MeV in light nuclei to a few tens of keV in rotational nuclei. These energy spacings decrease as one goes to higher excitation energies. As one can see from compound nuclear resonances observed with neutrons, near the separation energy the spacing is on the order of eV. To investigate reactions in which only a particular state of the final residual nuclei is excited, it is necessary to have a sufficiently good energy resolution, $\Delta E/E$, where ΔE is the effective uncertainty in our knowledge of the value of the energy. To observe states that are separated by the order of 10 keV, the value of $\Delta E/E$ for, say, a 10-MeV beam energy is on the order of 10^{-3}, while for 100 MeV it is 10^{-4} and for 1 GeV it is 10^{-5}. Eventually, as the level spacing becomes too small, it becomes impossible to resolve levels and one obtains cross sections that are averages over a number of levels.

Energy resolution is also required to observe resonances and other structure in the energy dependence of the cross section. Clearly, their unambiguous identification and their investigation become possible only if ΔE is less than the width of the resonance or, more generally, less than the range in energy over which interesting structure is present.

Energy resolution on the order of several parts in 10^5 has been achieved with primary beams of charged particles produced directly by accelerators. In Fig. 1.1 an extreme example is shown, demonstrating resolution on the order of 100 eV achieved for proton beams of about 2 MeV. Figure 1.2 illustrates an example of a similar resolution achieved with high-energy electron beams. Energy resolution of secondary beams of particles, such as neutrons, pions, and γ-rays, produced when a primary charged particle beam collides with nuclei, is steadily improving. The development of semiconductor detectors such as lithium-drifted germanium has been particularly useful for γ-ray detection (Fig. 1.3), while the development of electronics capable of picosecond timing has been of great value for the determination of neutron energies by the time-of-flight method. Better secondary beams and better precision can be obtained as well by increasing the intensity of the primary beam. Some facilities of this type have recently been built.

These improvements in the control of projectile beams and the detection of

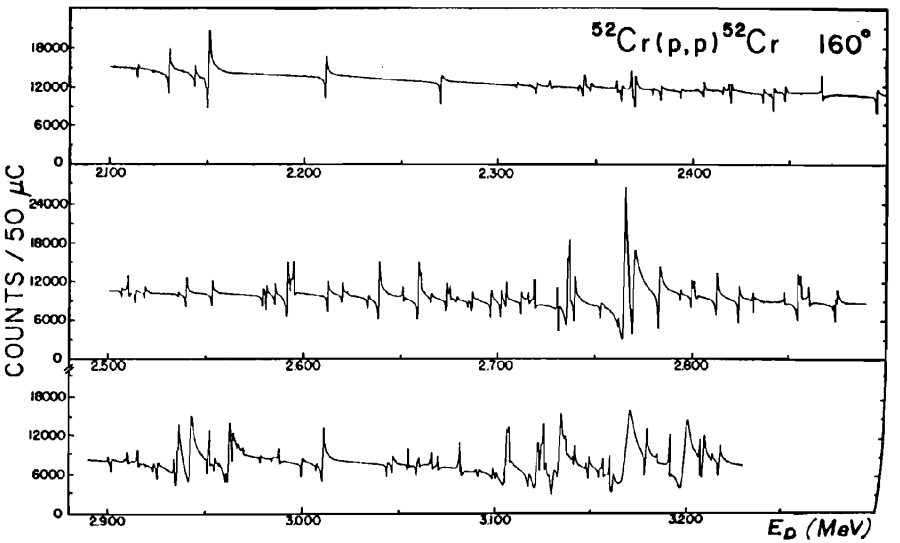

FIG. 1.1. High-energy resolution ($\Delta E \sim 100$ eV) achieved for proton beams for proton energies of a few MeV. [From Moses, Newson, et al. (71).]

reaction products make possible the discovery of relatively rare phenomena such as narrow isobaric analog resonance, observation of the structure of the broad giant electric dipole resonance (Fig. 1.4), and elucidation of nuclear structure as exemplified by the study of nuclei in the lead region, to cite a few examples.

A large variation in the energy of the projectiles, which has been substantially expanded in recent years, is possible, permitting the study of nuclear reactions under a variety of kinematic circumstances. For the most part (there are a few exceptions) the energies of projectiles employed have been less than a few GeV, although beams of nuclei with energies of 200 GeV per nucleon have recently become available.

Perhaps the most important insight to be gained from this discussion of the capabilities presently available to experimental nuclear physics is that they make it possible to conduct a systematic study of an entire class of phenomena, observing its dependence on the Z and A values and the structure of the target nucleus; the properties of the projectile, including its charge, mass, isospin, hypercharge, and structure; and on the projectile energy. Such multipronged investigations are necessary in strong interaction physics to unravel the various structural and dynamical elements determining the course of a reaction.

Nuclear theory plays an important role in this process. Its principal achievement in this regard has been to furnish a framework permitting a dynamical interpretation of the experimental data and the extraction of nuclear structure information. Calculations to predict nuclear reactions, based directly

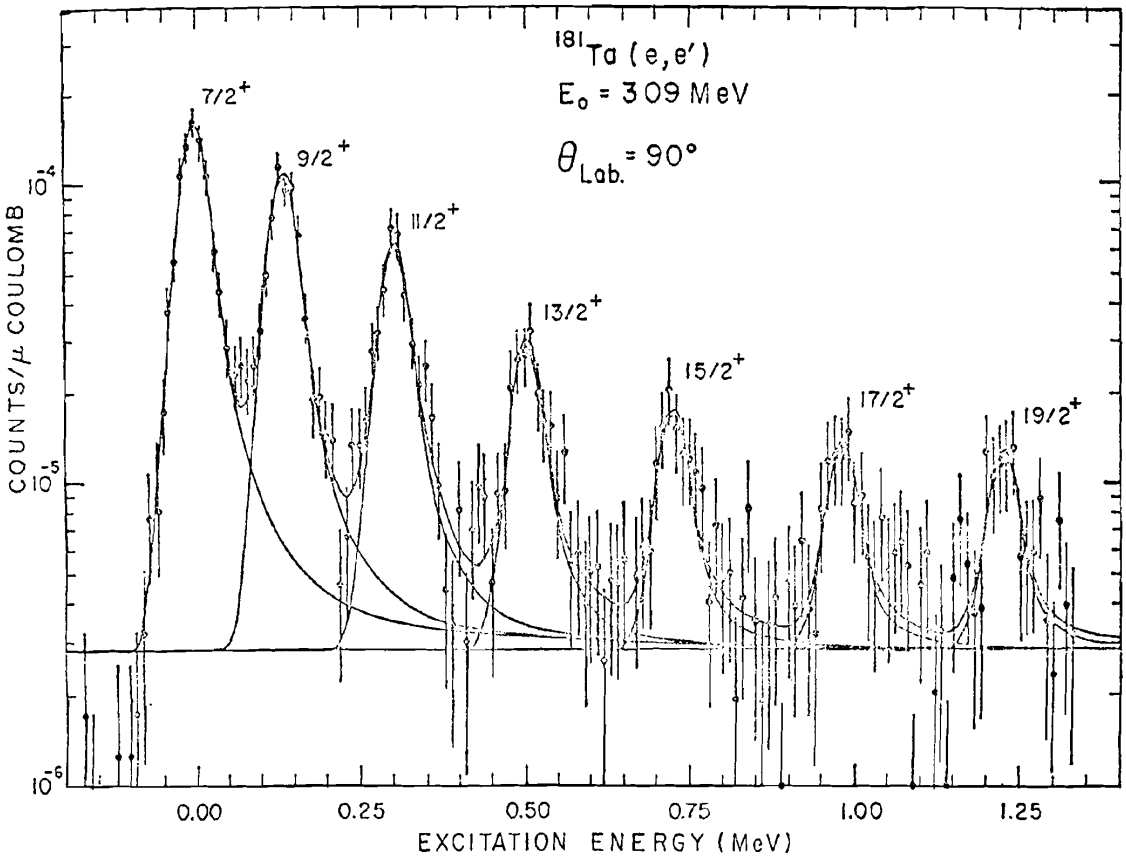

FIG. 1.2. High-energy resolution achieved with electron beams. [From Bertozzi (82).]

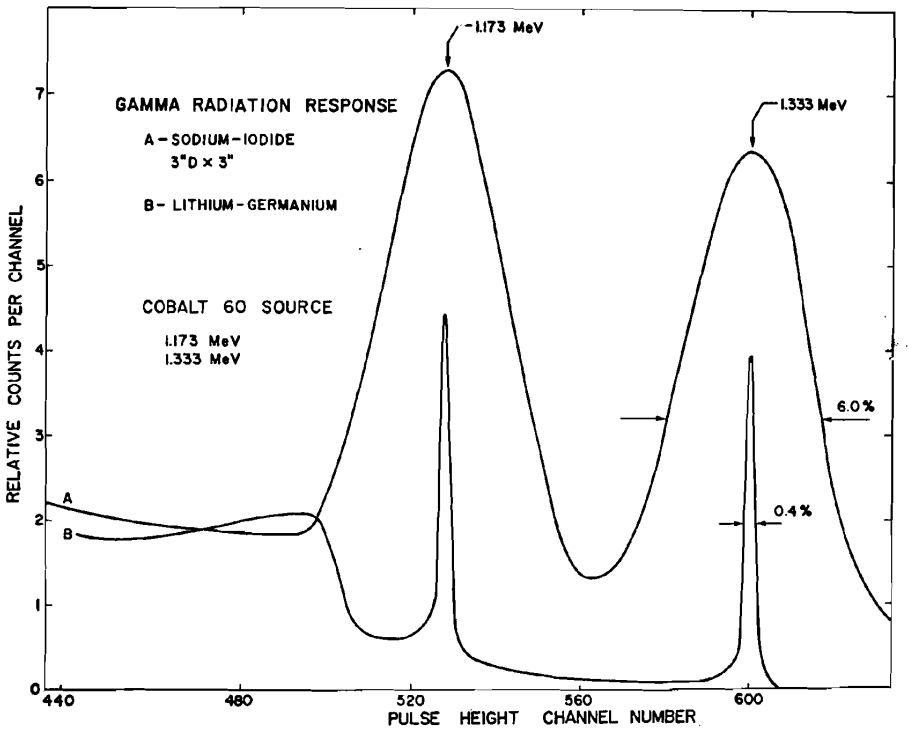

FIG. 1.3. Gamma-ray energy resolution obtained with (A) a sodium iodide detector and (B) a lithium–germanium detector. [(From Bromley).]

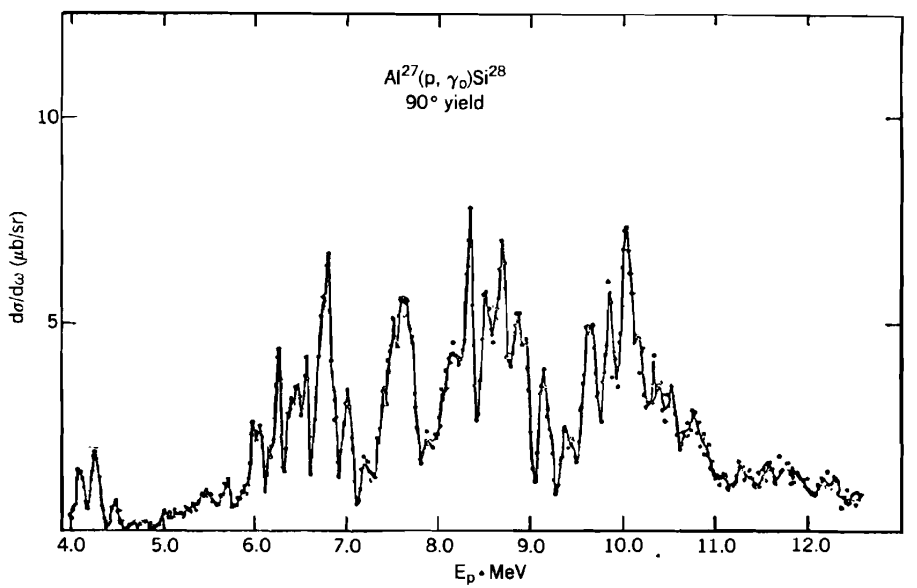

FIG. 1.4. Giant resonance structure. [From Singh, Segel, et al. (1965).]

on the underlying nucleon–nucleon forces, called the microscopic theory, have been rather few. However, as our understanding of the many-body problem grows, it may be expected that the methods used to predict the properties of nuclear matter and the low-lying states of finite nuclei will be extended to the "many-body problem in the continuum," which is just another way of describing nuclear reactions.

2. NOMENCLATURE AND ELEMENTARY KINEMATICS

Nuclear reactions involve the collision of an *incident projectile* with a *target nucleus.* As a consequence, the *initial system* is transformed into the *final system,* consisting of the *products of the reaction.* Symbolically,

$$a + X \rightarrow Y + b + c + \cdots \tag{2.1}$$

where a is the incident projectile, X the target nucleus, and Y the *residual nucleus.* A more succinct notation is often used: $X(a, bc, \ldots)Y$. The initial system is typically a two-body system. The target nucleus is in its ground state, while the incident projectile is generally stable or sufficiently long-lived. The final system may consist of several particles, so that one speaks of two-body, $X(a, b)Y$; three-body, $X(a, bc)Y$; and so on, final states. The residual nucleus or any of the emergent particles may be in its ground state, or it may be excited. The latter condition will be indicated by an asterisk.

The words *initial* and *final* describe the system when its constituents are spatially separated and noninteracting. The interacting system is referred to as the *compound system.* When the initial system is brought together so as to be interactive, it forms the compound system, which eventually comes apart into various possible final states. When a compound system lives a sufficiently long time so that it has well-defined quantum numbers such as energy, angular momentum, parity, and so on, the compound system is referred to as the *compound nucleus* and the corresponding long-lived state as the *compound nuclear state.*

In describing these reactions several conservation principles are employed. *Conservation of charge* and *baryon number* are directly applicable to the reaction equation, (2.1). The value of the total charge and the baryon number in the final state must equal their values in the initial state. The baryon number B is defined by the equation

$$B = A - \bar{A} \tag{2.2}$$

where A represents the number of baryons and $\bar{A}$ is the number of antibaryons. *Conservation of nucleons* is the special case of conservation of baryons appropriate for most nuclear reactions which do not usually involve strange particles or antibaryons. Generally, the baryon number and charge are known

for the initial system. Under these circumstances, observation of these numbers for a part of the final system (e.g., the emergent particles) immediately determines their values for the remainder of the system (e.g., the residual nucleus).

Conservation of charge and baryon number are considered absolute conservation principles, as indicated by the very long bounds to the lifetimes of the electron and proton. Moreover, the magnitudes of the charge of the electron and the proton are known to be equal to a very high accuracy. Other conservation rules are not as strongly obeyed. As has already been discussed in deShalit and Feshbach (74), because of the action of the electromagnetic field, isospin is not conserved. Hypercharge is not conserved in the weak interactions that induce the decay of strange particles, such as

$$\Lambda^0 \rightarrow p + \pi^-$$

However, it does appear to be conserved in the strong interactions. Violation of the *conservation of lepton number* [see deShalit and Feshbach (74), Chapter IX] has not been observed (e.g., the $\mu \rightarrow e + \gamma$ reaction has not been seen), but it is not as firmly established as the conservation of baryon number and charge.

Space–time symmetries and their corresponding conservation principles must also be preserved in nuclear reactions. Linear and angular momentum as well as energy are conserved. Parity is conserved and time-reversal invariance is valid for both the strong and electromagnetic interactions, which play the principal roles in nuclear reactions. The weak interactions, which lead to parity nonconservation in the hadron–hadron interaction [see deShalit and Feshbach (74), Chapter IX], or the neutral current of the Salam–Weinberg standard model, which leads to weak parity conservation violations in the electromagnetic interaction, have very little effect on nuclear reactions. Unless we are specifically investigating the weak interactions, there is no need to consider their effects.

There are some simple consequences of these invariance principles that it will be convenient to develop now. In most circumstances the target nucleus is stationary.‡ The colliding beams experiment, for which both the *target* and *projectile* are moving, is an exception. But so far this device has been used only for proton–proton, proton–antiproton, and electron–positron collisions. One can expect that heavy-ion colliding beams will become available in the future. The reference frame in which the target nucleus is at rest is referred to as the *laboratory frame.* Quantities associated with it will be designated by a subscript *L.*

From conservation of momentum we know that in the absence of any external forces the total momentum of the system is unchanged during collision and that its center of mass moves with a constant velocity. It is therefore convenient to use a uniformly moving coordinate system in which the center of mass is at rest. The position of the center of mass **R** with respect to an arbitrary reference

‡The target is, in fact, not at rest because of thermal motion. This is of importance for reactions induced by slow neutrons.

frame for a projectile of mass m and velocity $\mathbf{v}_1$ striking a target of mass M and velocity $\mathbf{v}_2$ is given nonrelativistically by

$$\mathbf{R} = \frac{m\mathbf{r}_1 + M\mathbf{r}_2}{m + M}$$

where $\mathbf{r}_1$ and $\mathbf{r}_2$ are the positions of the projectile and the target, respectively, with reference to some fixed origin. The velocity of the center of mass is

$$\mathbf{V} = \frac{m\mathbf{v}_1 + M\mathbf{v}_2}{m + M}$$

In the laboratory frame of reference ($v_2 = 0$)

$$\mathbf{V}_L = \frac{m\mathbf{v}_1}{m + M} = \frac{\mathbf{p}_L}{m + M} \tag{2.3}$$

where $\mathbf{p}_L$ is the momentum of the projectile. In the center-of-mass frame, $\mathbf{V} = 0$, so that $\mathbf{p}_1 = -\mathbf{p}_2$. Thus the center-of-mass frame can be referred to as a *zero-momentum frame*. The relations between the momentum and energy in the two frames, laboratory and zero-momentum, are needed. The two physical situations are compared in Fig. 2.1. In the figure, p is the common magnitude of $\mathbf{p}_1$ and $\mathbf{p}_2$. The center-of-mass frame is moving to the right with the velocity $\mathbf{V}_L$. Hence

$$\mathbf{p}_L = \mathbf{p} + m\mathbf{V}_L$$

or using (2.3),

$$\mathbf{p} = \frac{M}{m + M}\mathbf{p}_L \tag{2.4}$$

Thus the kinetic energy in the center-of-mass frame, E, and the kinetic energy

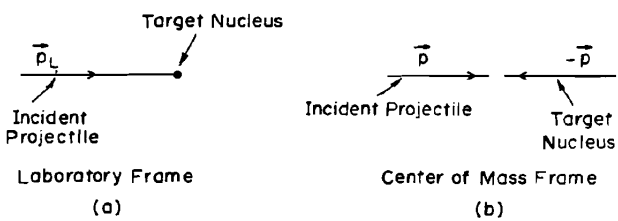

FIG. 2.1

in the laboratory frame, E_L, are related by

$$E = \frac{M}{m+M} E_L \tag{2.5}$$

Finally,

$$E = \frac{1}{2\mu} p^2 \tag{2.6}$$

where μ is the reduced mass:

$$\mu = \frac{Mm}{M+m}$$

The energy of the center of mass in the laboratory frame,

$$E_{cm} = \frac{m}{m+M} E_L$$

remains constant and is thus not available for the reaction.

The final and initial systems are related by the conservation principles. It is most useful at this point to discuss some of the consequences of the conservation of momentum and energy for two-body final states as illustrated in Fig. 2.2. The reaction is

$$a + X \rightarrow Y^* + b^*$$

where the asterisks indicate the possibility that the residual nucleus, Y, and the emergent particle, b, might be excited. In the center-of-mass frame, the energy

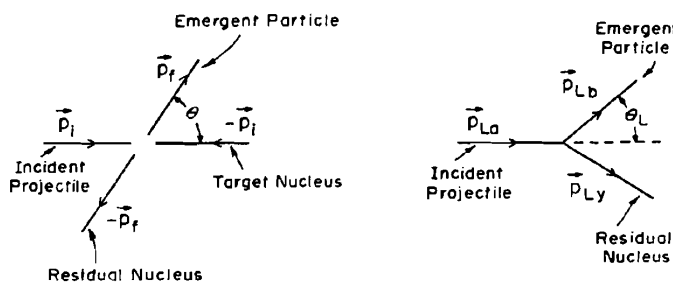

FIG. 2.2

of the initial system is, in the nonrelativistic limit, $(m_a + m_X)c^2 + T_i$, where the first two terms give the rest energy and T_i is the kinetic energy (2.6), with the momentum $\mathbf{p}$ equal to the initial momentum $\mathbf{p}_i$. The energy of the final system is, similarly,

$$(m_b + m_Y)c^2 + \varepsilon_b + \varepsilon_Y + T_f$$

where ε_b and ε_Y are the excitation energies of the particle b and nucleus Y, respectively. The value of the momentum p_f can be obtained from T_f using (2.6). Conservation of energy requires that the energies of the initial and final systems be equal. Hence

$$T_f - T_i \equiv Q_{fi} = (m_X + m_a - m_Y - m_b)c^2 - \varepsilon_b - \varepsilon_Y \tag{2.7}$$

where Q_{fi}, referred to as the *Q value*, gives the kinetic energy *released* by the reaction. If Q_{fi} is positive, the reaction will proceed even if T_i, the initial kinetic energy, is zero. The reaction is then said to be *exogeric*. If Q_{fi} is negative, T_i must at least equal $|Q_{fi}|$, the *threshold energy*, before the reaction can proceed. The reaction is then *endoergic*. In a typical case, the masses are known, and the emergent particle is not excited ($\varepsilon_b = 0$). Then by measuring Q_{fi} the value of ε_Y, the excitation energy of the residual nucleus, can be determined.

Of course, in practice, laboratory energies are measured directly and it sometimes is useful to express the energy difference $T_f - T_i$ as given by (2.7) in laboratory-frame variables. It is an easy matter to obtain Q_{fi} by applying conservation of momentum and energy in the laboratory frame. The result is

$$Q_{fi} = T_{Lb} + \frac{1}{2m_Y}(\mathbf{p}_{La} - \mathbf{p}_{Lb})^2 - T_{La} \tag{2.8}$$

or

$$Q_{fi} = \frac{1}{m_Y}[(m_Y + m_b)T_{Lb} - (m_Y - m_a)T_{La} - 2\sqrt{m_a m_b T_{La} T_{Lb}}\cos\theta_L] \tag{2.9}$$

where θ_L is defined in Fig. 2.2. The mass m_Y may be eliminated using its approximate value $m_X + m_a - m_b$. Since Q_{fi} depends only on intrinsic energies [see (2.7)], its value is independent of the angle θ_L. Thus T_{Lb} must vary with angle θ_L so as to cancel out the explicit θ_L dependence in the right-hand side of (2.9). The angle variation of T_{Lb} can be obtained from (2.9) by solving for T_{Lb} in terms of Q_{fi}.

3. CLASSIFICATION OF REACTIONS

Each of the projectiles can induce reactions of various kinds. We begin with the examples schematically illustrated in Fig. 3.1. This gives the energy spectrum

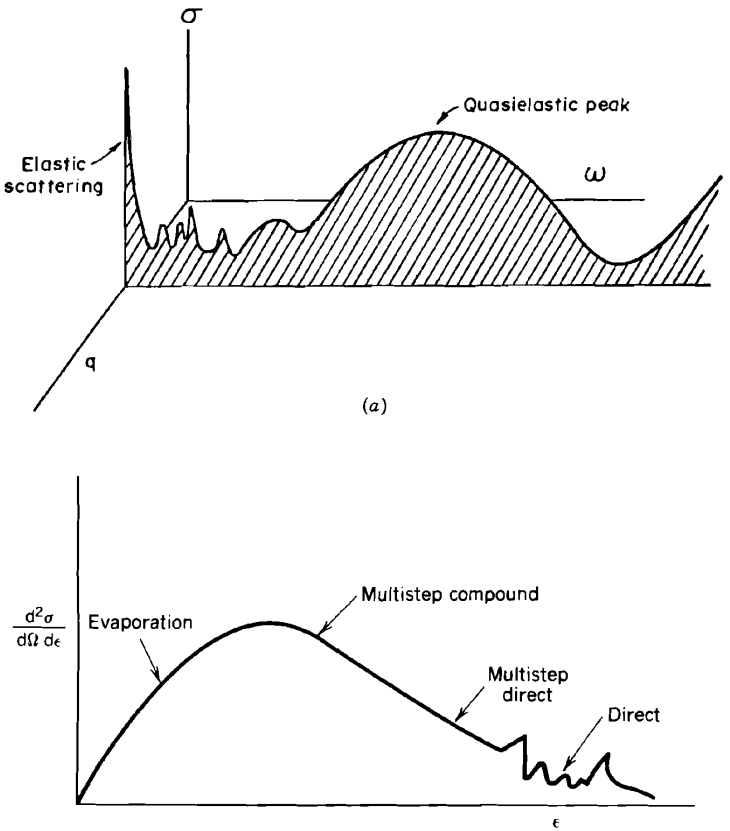

FIG. 3.1. (*a*) Energy spectrum of a particle scattered with a momentum transfer $\hbar q$ and an energy loss $\hbar\omega$; (*b*) energy spectrum of a nucleon emitted with an energy, ε, as the consequence of a reaction.

of a projectile scattered with a given momentum transfer $\hbar\mathbf{q}$ and energy transfer $\hbar\omega$ in the center-of-mass reference frame, where

$$\mathbf{q} = \mathbf{k}_i - \mathbf{k}_f \qquad \mathbf{p}_{i,f} = \hbar\mathbf{k}_{i,f} \tag{3.1}$$

and

$$\hbar\omega = E_i - E_f \tag{3.2}$$

where E_i and E_f are the energies of the target and residual nuclei, respectively. The peak in the intensity for zero energy loss is produced by *elastic scattering*, designated by $X(a, a)X$. Elastic scattering is defined to be a collision in which the colliding particles only change their direction of motion, and possibly spin

orientation if they have spin. None of the kinetic energy of the system is used to excite the colliding systems internally; that is, $Q_{fi} = 0$. The projectile and the target nucleus remain in their ground state, simply changing their direction of motion as illustrated in Fig. 3.2 but not the magnitudes of their momenta. The cosine of the angle of scattering, θ, is given by $\hat{\mathbf{k}}_i \cdot \hat{\mathbf{k}}_f$. It is related to $\mathbf{q}$ as follows:

$$q = 2k \sin \tfrac{1}{2}\theta \tag{3.3}$$

where k is the common magnitude of $\mathbf{k}_i$ and $\mathbf{k}_f$.

If both or either the projectile and target nucleus are complex, *inelastic scattering* can occur with the excitation of either or both, as indicated by $X(a, a^*)X^*$. The reaction is endoergic. The sharp peaks for nonzero values of ω in Fig. 3.1*a* correspond to the excitation of sharp discrete levels in, for example, the target nucleus. Figure 3.2 still applies, but in contrast to elastic scattering, p_i no longer equals p_f. The energy transfer $\hbar\omega$ equals the excitation energy ε, so that

$$\hbar\omega \equiv \varepsilon = \frac{1}{2m}(p_i^2 - p_f^2) \tag{3.4}$$

where it has been assumed that the change in the kinetic energies of the target can be neglected. Relation (3.3) is replaced by

$$q^2 = (k_i - k_f)^2 + 4k_i k_f \sin^2 \tfrac{1}{2}\theta \tag{3.5}$$

Since ε is fixed, the magnitude of k_f does not vary with angle. However, the value of q, for a given ε, does vary with angle, increasing as θ increases. The significance of q can be seen from the Born approximation, which states that the amplitude for the process will be proportional to

$$\int e^{-i\mathbf{k}_f \cdot \mathbf{r}} V(\mathbf{r}) e^{i\mathbf{k}_i \cdot \mathbf{r}} d\mathbf{r} = \int e^{i\mathbf{q}\cdot\mathbf{r}} V(\mathbf{r})\, d\mathbf{r}$$

where V is the effective potential which induces the transition, elastic or inelastic as the case may be. V will generally depend on the properties of the nuclear systems undergoing the transition. We see that the reaction will serve as a probe

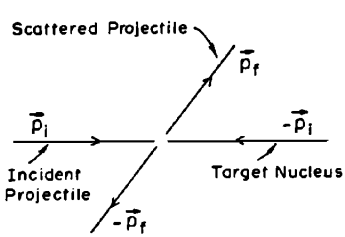

FIG. 3.2

of $V(r)$ for distances on the order of $\hbar/q$. Thus the larger the q, the more sharply the short-range properties of V are probed.

For larger energy transfers (Fig. 3.1*b*), the spectra lose their discrete character and become continuous. For one thing the density of levels of the target nucleus becomes so large that it is no longer possible to distinguish individual levels. It should also be realized that the approach to the continuous energy spectrum will differ with differing types of excitation. States of the excited nucleus with high angular momentum, J, will, for example, achieve the requisite high-level density at comparatively high excitation energies. At the lower energies the spectrum may thus be, effectively continuous as far as small values of J are concerned but will have a superimposed discrete character characterized by large values of J.

For sufficiently large energy transfers, those exceeding the separation energy for a nucleon, deuteron, or other fragments, the target nucleus can emit a particle,. The corresponding reactions are referred to as $(p, 2p)$, $(p, p'd)$, and $(p, p'\alpha)$ when the incident particle is a proton. The final states consist of the residual nucleus; the incident proton, which has lost energy; and the particle, which has been knocked out of the target nucleus—and are thus at least three-body final states.

An important feature in this regime is a consequence of the *quasi-elastic scattering mechanism.* In quasi-elastic scattering the incident particle is assumed to collide elastically with a nucleon (or a complex cluster) within the target nucleus, the remainder of the target nucleus acting as a "spectator." If the nucleons (or clusters) in the nucleus were at rest and free, one would see a sharp peak in the cross section at an energy loss, $\hbar\omega$, corresponding to the energy acquired by the nuclear nucleons. Using definitions (3.1) and (3.2), this implies that

$$\hbar\omega = \frac{\hbar^2 q^2}{2m} \tag{3.6}$$

where m is the mass of the nuclear nucleons (or clusters).

However, the nucleons in the nucleus move with a momentum p. In a Fermi-gas model the maximum value of p is p_F, the Fermi momentum. The conservation of momentum requires that the momentum $\hbar\mathbf{q}$ [see (3.1)] lost by the incident particle is acquired by the target nuclear nucleon of mass m^*, where m^* the effective mass, is a function of the momentum, taking into account to some extent the effect of the interaction with other nucleons in the nucleus. Therefore, more accurately,

$$\frac{p^2}{2m^*(p)} + \hbar\omega = \frac{P^2}{2m^*(P)} \qquad \mathbf{P} = \mathbf{p} + \hbar\mathbf{q} \tag{3.7}$$

This equation neglects the recoil energy of the residual nucleus, whose maximum value is on the order of $\varepsilon_F/(A-1)$, where A is the mass number of the target

nucleus and ε_F is the Fermi energy. This approximation is valid only when $\hbar\omega$ and $\hbar q$ are sufficiently large. From (3.7) one obtains a relation between ω and q, neglecting the difference between $m^*(p)$ and $m^*(P)$:

$$\hbar\omega = \frac{1}{m^*}\left(\hbar\mathbf{p}\cdot\mathbf{q} + \frac{\hbar^2 q^2}{2}\right) \tag{3.8}$$

Hence $\hbar\omega$ is bounded as follows:

$$\frac{p_F\hbar q}{m^*} + \frac{\hbar^2 q^2}{2m^*} > \hbar\omega > \frac{-p_F\hbar q}{m^*} + \frac{\hbar^2 q^2}{2m^*} \tag{3.9}$$

The free nucleon peak at $(\hbar q)^2/2m$ is shifted to $\hbar^2 q^2/2m^*$. Moreover, it spreads out, acquiring a width of the order of $\hbar p_F q/m^*$ as a consequence of the internal motion of the nucleons of the target nucleus. It should be noted that the peak energy depends on the angle θ between the initial and final momenta, $\mathbf{p}_i$ and $\mathbf{p}_f$, in a characteristic way. This fact can be used to differentiate the quasi-elastic peak from others. The energy difference $\hbar\omega = Q_{fi}$ for inelastic excitation, for example, does not vary with the center-of-mass angle θ [see (2.7)].

Problem. Discuss how these conclusions are changed because of a possible difference between $m^*(p)$ and $m^*(P)$.

The presence of the quasi-elastic peak is shown in Fig. 3.1a. Its shape depends, at least in the noninteracting Fermi-gas or shell model, on the distribution of momenta within the nucleus or more generally on the state of the struck particle. The energy of the emergent particle is not given by $p^2/2m^*$ since that is its energy relative to the bottom of the potential well, as shown in Fig. 3.3. The observed energy is $p^2/2m^* - \varepsilon_b$, where ε_b is the binding energy, the minimum energy required to remove the struck nucleon from the nucleus.

Some experimental results for the $(e, e'X)$ cross section, in which only the inclusive cross section in which only the emerging electron and not X is observed, are shown in Fig. 3.4. The solid lines give the fit obtained with the quasi-elastic mechanism using the Fermi-gas model of the target nucleus. The values of ε_b

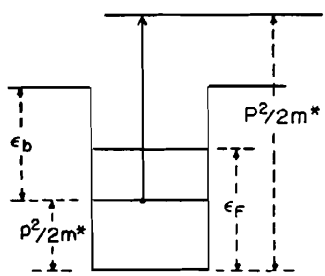

FIG. 3.3. Quasi-elastic scattering.

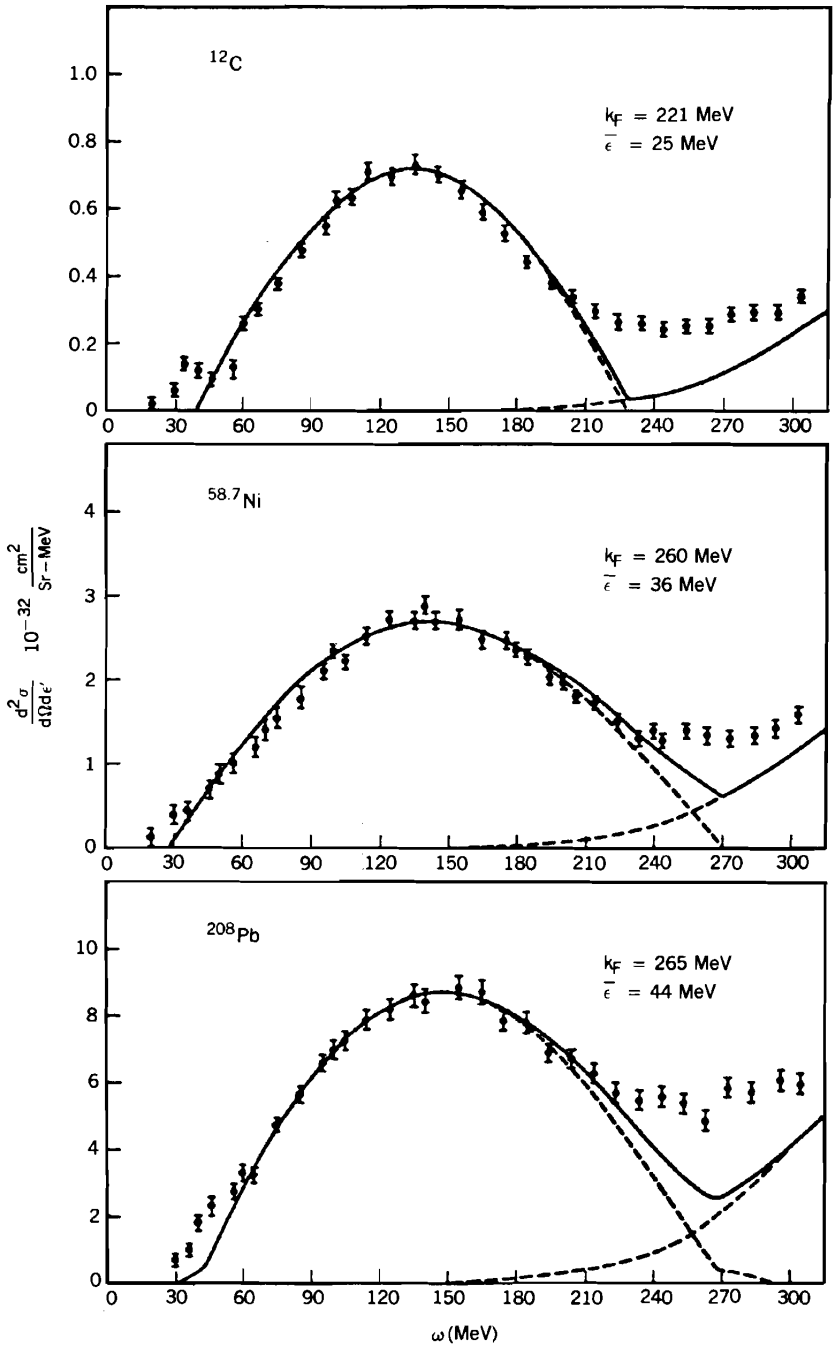

FIG. 3.4. Quasi-elastic scattering of electrons. The solid lines are calculated using a Fermi-gas nuclear model. [From Moniz et al. (71).]

and p_F are indicated in the figure and are also given in Table I.15.1 in deShalit and Feshbach (74).

More information can be obtained if the emergent proton in the (e, ep) and $(p, 2p)$ reactions are also detected in a coincidence experiment. In these experiments it becomes possible to determine ε_p for different single-particle orbitals and to obtain information on the momentum distributions for each.

In Figs 3.1a and 3.4, note the minimum at the low-$\hbar\omega$ end of the inelastic spectrum, lying between the quasi-elastic peak and the region where discrete levels are excited. This minimum is a consequence of the competition with the many other reactions that can occur in this region. At the upper end of the peak, we see that the spectrum shows a rise that is not predicted by the Fermi-gas model. This is a consequence of pion production.

Reactions in which the residual nuclei differ in either their mass number A, atomic number Z, or hypercharge Y, are called *transmutations*. When the mass number does not change but the atomic number or hypercharge do change, the reactions are referred to as *charge exchange* (CEX) or *hypercharge exchange scattering* (HCEX). Examples of charge exchange reactions include the (p, n), the $(^3\text{He}, ^3\text{H})$, and so on, reactions. With pion projectiles one can observe both single and double charge exchange reactions,

$$\pi^{\pm} + (Z, A) \rightarrow \pi^0 + (Z \pm 1, A)$$
$$\pi^{\pm} + (Z, A) \rightarrow \pi^{\mp} + (Z \pm 2, A)$$

where (Z, A) denotes a nucleus with atomic number Z and mass number A. The second of these reactions can lead to nuclei relatively far from the "stable" valley. For example, if the target is ^{16}O, the resulting nucleus produced by the double charge exchange reaction (π^+, π^-) is ^{16}Ne.

Hypercharge exchange reactions can involve either incident kaons or the production of kaons. In the first the hypercharge of the kaon is transferred to a nucleon in the target converting, for example, a neutron into a Λ. For example,

$$K^- + {}^{12}\text{C} \rightarrow {}^{12}_{\Lambda}\text{C} + \pi^-$$

where ${}^{12}_{\Lambda}\text{C}$ consists of six protons, five neutrons, and one lambda and is referred to as a hypernucleus. Associated production can also lead to hypercharge exchange. The elementary processes can be

$$\pi^+ + n \rightarrow K^+ + \Lambda$$
$$\rightarrow K^+ + \Sigma^0$$
$$\text{etc.}$$

The nuclear process corresponding to the first of these reactions is, for example,

$$\pi^+ + {}^{12}\text{C} \rightarrow {}^{12}_{\Lambda}\text{C} + K^+$$

Particle transfer reactions form a most important class of reactions leading to transmutations. The stripping (d, p) and pickup reactions (p, d) in which a neutron is transferred to or from the target nucleus played an important role in establishing the nuclear shell model. The (d, p) reaction was found to populate the single-particle neutron shell model states selectively, while the (p, d) reaction was found to be sensitive to the orbital of the neutron, which is "picked up" to form the deuteron. It proved possible in both these cases to correlate the angular distributions of the protons or deuterons in the two cases with the properties of the single-particle orbital from or to which the neutron is transferred. In Fig. 3.5 the values of l labelling each curve indicate the orbital angular momentum in question. As is apparent, the value of l can be deduced immediately from the shape of the angular distribution. Single proton transfer reactions with deuterons such as the (n, d) or (d, n) reactions are most difficult since at least until recently, neutrons have proven to be more difficult to manage. It has been necessary to turn to reactions with ^{3}He, such as the $(^3\text{He}, d)$ or $(d, ^3\text{He})$ to investigate single proton transfer reactions.

The transfer of two neutrons is studied in the $(^3\text{H}, p)$ and (p, H^3) reactions. In this case it is believed that the two neutrons transferred are in a $^1S_0$ state since that is for the most part their state within the ^{3}H nucleus. It may be expected that the pickup reaction $(p, ^3\text{H})$ reactions will proceed most vigorously when the target nucleus ground state is superconducting, being built up of precisely such correlated pairs. An example is shown in Table 3.1. This reaction is clearly useful for the discovery and study of pairing correlations.

Reactions in which a larger number of nucleons are transferred have been observed using α-particles and most recently, heavy-ion projectiles. The transfer of as many as eight nucleons has been seen; in this way the production of many new nuclei away from the stable valley has become possible.

Still another class of reactions occurs when the incident projectile is a boson. When the projectile is a photon, a pion, or a kaon, it can be absorbed by the target nucleus. This process, referred to as *absorption*, can result in the transfer of a relatively large amount of energy but with a relatively small amount of momentum transfer. This is obvious in the case of photon absorption. In that case the absorption by a single nucleon of the target nucleus is reduced since the recoil energy of the nucleon $\hbar^2\omega^2/2mc^2$ is very small compared to the energy transfer $\hbar\omega$ for photon energies $\hbar\omega \ll mc^2$. As a result, the absorption is by a pair of nucleons in which the nucleons move in antiparallel directions so that their energy can be appreciable while their net momentum is small. A similar phenomenon can occur when pions and (to some extent) kaons have small momentum, as in the case of pionic and kaonic atoms, in which π^- and K^- are captured in atomic orbits by the attractive Coulomb field of the nucleus. In that situation the momentum of the pion or kaon is small, while upon absorption by the nucleus, an energy equal to $m_\pi c^2$ or $m_K c^2$ is released. In the case of kaon absorption there is a finite probability that a hypernucleus is formed. Indeed, it was through this process that the first hypernuclei were observed.

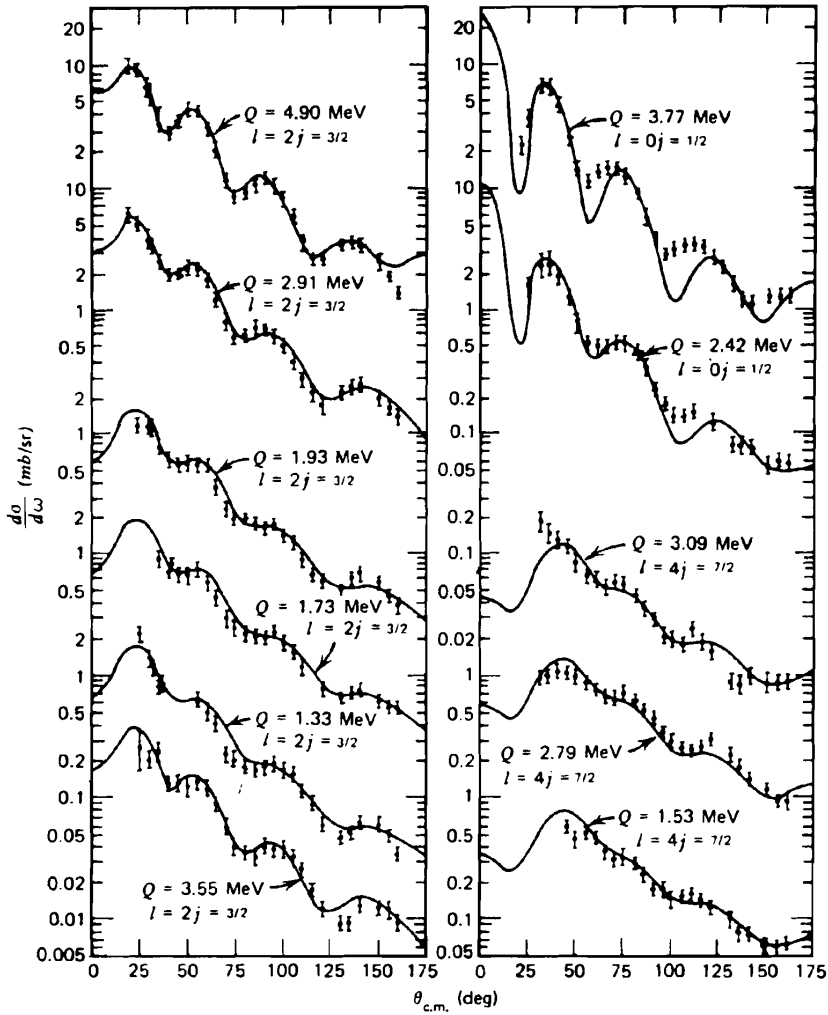

FIG. 3.5. Angular distribution for the $^{90}Zr(d,p)$ reaction with 12-MeV deuterons in which the neutron transferred to ^{90}Zr carries an orbital angular momentum of $l = 0, 2, 4$. [From Satchler (66).]

Photon absorption with the emission of a single nucleon [e.g., (γ, n)] also occurs. The underlying process may be the two-nucleon absorption, with one nucleon captured before it emerges from the nucleus. Of course, this capture *must* occur if the photon energy is below the threshold for the production of two nucleons. In that event it may become more convenient to describe the process as the excitation of the target nucleus into the continuum. The effect of the other nucleons is then contained in the high-momentum components of the single-particle wave function of the absorbing nucleon.

TABLE 3.1 Yield Y for the $^{124}Sn(t,p)$ Reaction Forming ^{126}Sn[a]

(t,p) group	E_n (MeV)	L	Y
0	0	0	100
1	1.164	2	5
2	2.070	>2	3
3	2.185		4
4	2.236		7
5	2.377		5
6	2.659		2
7	2.732		6
8	2.905		3
9	3.439		4
10	5.226		4
11	5.282		9
12	5.313		11
13	5.762		10

Source: (Bjerregaard Hansen, et al. (69)).

[a]L is the transferred angular momentum.

The inverse of photon absorption is called *radiative capture*, such as (n,γ), (p,γ), (π,γ) and so on. The neutron capture process, for example, is very useful for determining the presence and properties of low-lying levels of the final nucleus, which are readily connected via the electromagnetic interaction to the capturing energy region. In the neutron case, the first step in the capture of the neutron can be the formation of a compound nuclear resonance. In the proton case, the use of polarized protons[‡] in the $(\mathbf{p},\gamma)$ reaction has led to a more complete understanding of the contribution of the various multipole momenta in the giant dipole resonance region.

Fermions can be absorbed by the nucleus through the weak interactions. For the electron the process is known as K, L, and so on, capture and results in neutrino emission [see deShalit and Feshbach (74), Section IX.6]. In the case of muons [see deShalit and Feshbach (74), Section IX.18], the final state can consist of the muon neutrino and a nucleon as well, because of the large rest-mass energy of the muon.

Absorption of antiparticles such as the antiproton, $\bar{p}$, proceeds through the strong interactions for the most part. In the case of antiprotonic atoms in which the antiproton is in an atomic orbit about the attractive Coulomb field of the nucleus, absorption of the antiproton involves the *annihilation* process. The

[‡]Polarized projectiles are indicated by boldface.

important elementary process is

$$\bar{p} + p \rightarrow (n\pi)$$

where $(n\pi)$ refers to the emission of n pions. The analogous electromagnetic system, positronium, decays by the emission of photons:

$$e^+ + e^- \rightarrow (n\gamma)$$

where n is 2 or 3, depending on the state of the positronium. Larger values of n are not easily observable because of the weakness of the electromagnetic interaction.

The inverse of boson absorption is boson *production.* When protons of sufficient energy strike a nucleus, pions can be produced, as exemplified by the reaction

$$p + (Z, A) \rightarrow (Z, A + 1) + \pi^+ \tag{3.10}$$

The threshold for this process occurs at a lower energy than the elementary processes:

$$p + p \rightarrow n + p + \pi^+$$
$$\rightarrow d + \pi^+$$

For the first of these the kinetic energy in the center-of-mass frame is $\frac{1}{2}E_L$, whereas, with the nuclear target the kinetic energy in the same frame is $[A/(A+1)]E_L$. Roughly (neglecting differences in the neutron and proton masses, etc.), E_L for the p–p reaction must be at least $2m_\pi c^2$, while for the nuclear target the threshold energy $[1 + (1/A)]m_\pi c^2$ is considerably less. However, the cross section will be very small in this limit, since the entire target nucleus must be involved in the collision and production process. Intuitively, one would expect that the critical parameter is the ratio of the momentum transfer, $\hbar q$, to the Fermi momentum p_F. If this ratio is greater than 1, the probability of ejecting a nucleon will be correspondingly large and the probability of (3.10) occurring is reduced. If the produced pion is at rest, and if one neglects the momentum of the neutron added to the target nucleus by the reaction, this ratio becomes p_L/p_F, where p_L is the momentum of the incident proton in the laboratory frame. At threshold, nonrelativistically,

$$\frac{p_L}{p_F} = \sqrt{\frac{2mm_\pi Ac^2}{(A+1)p_F^2}} \approx 2\sqrt{\frac{A}{A+1}}$$

Since this ratio is greater than 1 for all nuclei, there will be a reduction in the cross section of process (3.10). Indeed, as soon as it becomes energetically

possible, the reaction

$$p + (Z, A) \rightarrow (Z, A) + p + \pi$$

is expected to dominate.

When the energy deposited in a nucleus is sufficiently large, as can be the case if the incident projectile is very energetic, or when the nucleus absorbs a massive particle as described above, the nucleus may break apart into several highly excited large fragments. This catastrophic event is referred to as *fragmentation*. In response to relatively minor perturbations, heavy nuclei whose stability is reduced by the repulsive electrostatic forces will fragment into two

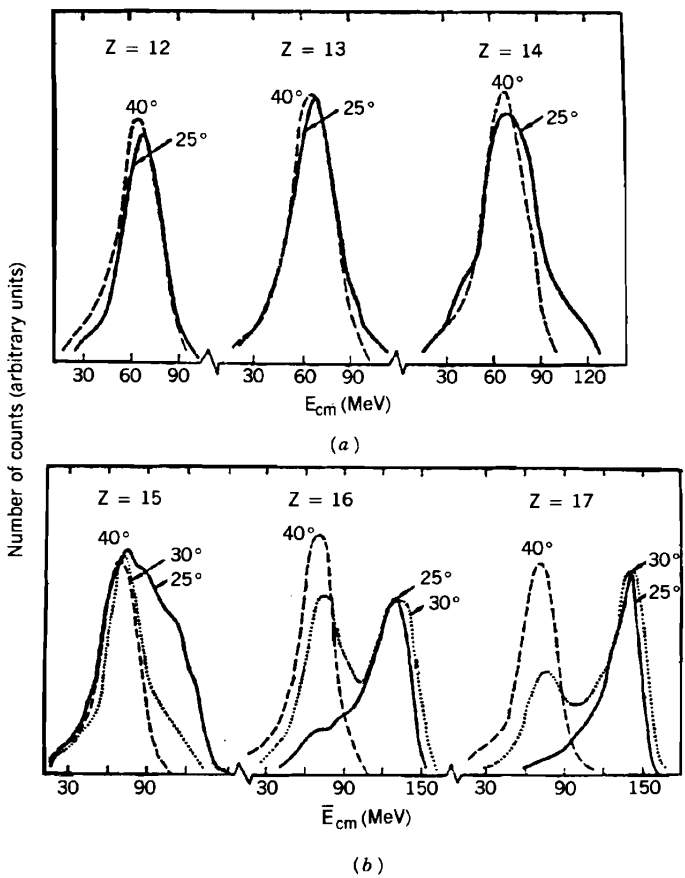

FIG. 3.6. Energy distribution of the light products in the reaction (^{40}Ar + ^{108}Ag): (*a*) for $Z = 12$, 13, and 14 the spectra are identical at 25° and 40°; (*b*) for $Z = 15$, 16, and 17, the deep inelastic process appears more clearly at 40°. [From Lefort (76).]

or more massive fragements. This process is called *fission. Fusion* is an inverse process in which heavy ions combine to form a single nucleus with perhaps the emission of a few light particles. Recently, a process termed *deep inelastic collision* has been discovered. It is found that in the process most of the kinetic energy available in the initial system has been transformed into internal energy. The observed kinetic energy of the final system is mostly a consequence of Coulomb repulsion. That is, it can be understood to be equal to the Coulomb energy of the two emerging nuclei making up the final system, in contact and at rest. As an example, consider the reaction ${}^{40}_{18}\mathrm{Ar} + {}^{108}_{47}\mathrm{Ag}$; the energy of the argon projectile is 288 MeV. In Fig. 3.6 we plot the energy distribution of the fragments $Z = 12$, 13, and 14 at two angles, 25° and 40°. It will be seen that the energy distribution at the two angles for the various fragments is nearly identical! This is the signature for this remarkable phenomenon. The peak energy is about 72 MeV. Assuming a two-particle final state, the total energy of the final system is 78 MeV, considerably less than the 288 MeV and reasonably close to the Coulomb energy of the two final particles.

4. DIRECT AND COMPOUND NUCLEAR REACTIONS

The various processes discussed just above can proceed through a variety of mechanisms. An early differentiation was made between "direct" and compound nuclear statistical reactions. In Sections I.12 and I.13 of deShalit and Feshbach (74) it was emphasized that the two reaction types, the direct and that leading to the formation of a compound nuclear state, could be distinguished by the time delay caused by the reaction or equivalently, by the interaction time required for the completion of the reaction. The direct reaction involves a short time delay whose order of magnitude is the time it would take a projectile and/or the emergent particle simply to traverse the nucleus. As pointed out in deShalit and Feshbach (74), a short time delay is reflected in a relatively weak dependence of the cross section on energy as well as a strongly anisotropic angular distribution, indicating that the memory of the direction of motion of the projectile has not been lost in the course of the reaction. In other words, from the angular distribution it is possible to estimate the direction of motion of the incident projectile. These properties of direct reaction have led to the *single-step* description of the process referred to as the *DWA distorted wave approximation* (DWA). In a single-step process, the projectile (e.g., a proton) in *one interaction* forms the emergent particle (e.g., a deuteron). The matrix element for this process (p,d) is therefore written as a matrix element of the effective transition potential, V, acting directly on the initial state to produce the final state. If the process is $X(a,b)Y$, the initial-state vector is the product of a state vector $|a, X\rangle$, giving the dependence on the internal variables of projectile a and the target nucleus X, and the wave function $\chi_i^{(+)}(\mathbf{k}_i, \mathbf{r})$, giving the dependence on their relative coordinate $\mathbf{r}$ with $\hbar\mathbf{k}_i$, the incident momentum. $\chi_i^{(+)}$ is a "distorted" wave in that it is not a plane wave but also takes into account the

average interaction between the projectile and the target.‡ The plus superscript denotes the outgoing diverging wave boundary conditions satisfied by $\chi_i^{(+)}$. In terms of this description of the initial state and an analogous one for the final state, the DWA matrix element giving the amplitude for a direct reaction is proportional to

$$\int d\mathbf{r}[\chi_f^{(-)}(\mathbf{k}_f, \mathbf{r})]^+ \langle b, Y | V | a, X \rangle \chi_i^{(+)}(\mathbf{k}_i, \mathbf{r}) \tag{4.1}$$

In this equation $\chi_f^{(-)}$ is the wave-function describing the relative motion of the final constituents, subject to the converging wave boundary condition. In the $X(p,d)Y$ case, $\chi_i^{(+)}$ describes the dependence on the relative p–X coordinate, while $\chi_f^{(-)}$ is the wave function for the dependence on the relative d–Y coordinate. The single-step nature of the process is indicated by the linear dependence of the matrix element on the potential, V. This "theory" can give excellent agreement with the appropriate experiment, as exemplified by Fig. I.12.1 in deShalit and Feshbach (74).

The compound nuclear resonance involves a very long interaction time, as can be seen directly from the very rapid variation of the cross section with energy, as indicated by its width, Γ [see Fig. I.12.3 in deShalit and Feshbach (74)]. The resonance demonstrates the presence of a nearly bound state of the compound nucleus, with well-defined quantum numbers such as energy, angular momentum, and parity—the compound nuclear state, whose lifetime is given by $(\hbar/\Gamma)$. Clearly, the excitation of the compound nucleus state cannot be described in terms of a single-step process. Rather, the incident projectile completely loses its identity, amalgamating with the target nucleus to form a compound nuclear state. The compound nuclear state lives for a finite (rather than an infinite) time because it can decay by emitting a variety of products. If the particle emitted is identical with the incident projectile, the process is elastic or inelastic scattering. If the particle emitted is *not* identical with the incident projectile, the reaction is a transmutation. If interference with the direct reaction is unimportant, the angular distribution of a reaction product is symmetrical about 90°. It is thus no longer possible to ascertain the direction of motion of the incident projectile, although its line of motion is determined.

The isolated compound nuclear resonance is a spectacular phenomenon. However, it can be observed in only a comparatively limited energy range. As soon as the excitation energy increases sufficiently, the density of resonances and the variety of accessible exit channels will become so large that it becomes most unlikely that an isolated compound nuclear resonance will be present. Rather, the resonances will overlap, their presence being reflected by fluctuations in the energy dependence of the cross section away from a smooth average. In this regime it becomes necessary to use statistical measures such as averages

‡The quantities, the effective transition potential, and the average projectile–target nucleus interaction are discussed and described in Chapter VI.

over the fluctuations and mean-square deviations from the average. This theory is referred to as the *statistical theory of compound nuclear reactions.*

The principal assumption of this theory rests on the insight that the wave function for the system is very complex, consisting of a large number of components (e.g., the overlapping resonances). The amplitudes, both in magnitude and phase, of each of these vary rapidly as the energy changes. The assumption is made that these amplitudes are random variables. The expression for the reaction cross section, depending on the square magnitude of reaction amplitude, will therefore depend on bilinear products of this set of random variables. Upon averaging, the cross products of the random variables will vanish. This result follows from the assumption that the phase of each component amplitude is random. We provide a detailed discussion of the consequences of this approach in Chapter IV.

Problem. Let $f = \sum_{n,m} A_n(E_i)B_m(E_f)$, where A_n and B_m are random variables. Show that $\langle |f|^2 \rangle = [\sum_n |A_n(E_i)|^2][\sum_m |B_m(E_f)|^2]$.

For the present purposes it will suffice to quote the results that follow exactly for the collision of spinless systems producing spinless reaction products, and that follow approximately for reactions involving particles with spin. The average cross section for exciting a specific level in the residual nucleus is

$$\langle \sigma_{if}(E_f) \rangle = \sigma_c(i; E_i) \frac{A_f(E_f)}{\sum_a A_a(E_a)} \tag{4.2}$$

This result is an expression of the *Bohr independence hypothesis.* The cross section factors into two terms. The first, $\sigma_c(i; E_i)$, gives the cross section for forming the compound system when the available center-of-mass energy is E_i and the quantum numbers describing the target nucleus are symbolized by i. The second factor, depending only on the final energy, is a branching ratio giving the probability that the compound nucleus will decay to a particular final state.

An approximate argument (which turns out to yield the correct result!) provides the form for A_f. A more precise discussion is given in Chapter IV. We assume incorrectly (why?) that detailed balance is valid for the reaction considered above. For spinless systems, detailed balance states that

$$E_i \langle \sigma_{if}(E_f) \rangle = E_f \langle \sigma_{fi}(E_i) \rangle \tag{4.3}$$

Inserting (4.2) into this equation yields

$$A_f(E_f) \sim E_f \sigma_c(f; E_f)$$

Hence

$$\langle \sigma_{if}(E_f) \rangle = \frac{\sigma_c(i; E_i) E_f \sigma_c(f; E_f)}{\sum_a E_a \sigma_c(a; E_a \rangle} \tag{4.4}$$

Generally, in the energy region where this formula is to be applied, the final states of the residual nucleus form a continuum, or the individual states are not resolvable. Suppose that the density of states at the excitation energy of the residual nucleus U_{fi} is $\omega_0(U_{fi})$. Then the spectrum $\langle d\sigma_{if}/dE_f \rangle$ is given by

$$\left\langle \frac{d\sigma_{if}}{dE_f} \right\rangle = \sigma_c(i; E_i) \frac{\mu_f E_f \sigma_c(f; E_f) \omega_0(U_{fi})}{\sum_a \mu_a \int dE_a E_a \sigma_c(a; E_a) \omega_0(U_{ai})} \tag{4.5}$$

where μ_a is the reduced mass for the possible final systems. This formula applies approximately to systems with spin if ω_0 is the density of levels with zero total spin. The value of the excitation energy, U_{fi}, is given by

$$U_{fi} = E_i + Q_{fi} - E_f \tag{4.6}$$

where Q_{fi} is the Q of the reaction [see (2.7)].

Despite the approximations involved in deriving (4.5), it has proved to be of great utility, in part because it gives a very definite prescription for determining an average cross section. The cross section for forming the compound nucleus can readily be calculated from the optical model obtained from fitting elastic scattering cross sections and angular distributions. In the short-wavelength limit for a strongly absorbing nucleus and a neutral projectile, it is given roughly by $\pi R^2(1 - \langle V \rangle / E)$, where R is the *nuclear radius*, that is, the radius of the potential acting between the target (residual nuclus) and the projectile (emitted particle) and $\langle V \rangle$ is the average strength of that potential.

Some consequences of (4.5) are immediately clear. The ratio

$$\frac{d\sigma_{if}/dE_f}{\sigma_c(i; E_i) E_f \sigma_c(f; E_f)}$$

depends only on the excitation energy U_{fi}, that is, only on the difference $E_i - E_f$ and not on either E_i and E_f separately. This assumes that the denominator on the right-hand side of (4.5) is insensitive to E_i. This is to be expected when there are many channels into which the compound system can decay. Moreover, it is possible to extract the level density ω_0, which is traditionally (Chapter IV) parametrized as follows:

$$\omega_0(U) = Ce^{2\sqrt{aU}} \tag{4.7}$$

The empirical values of a for a number of nuclei are shown in Fig. 4.1. As one can see, the density of states rises very rapidly as the excitation energy U increases.

The function $\omega_0(U)$, where U is given by (4.6), can be expanded about the

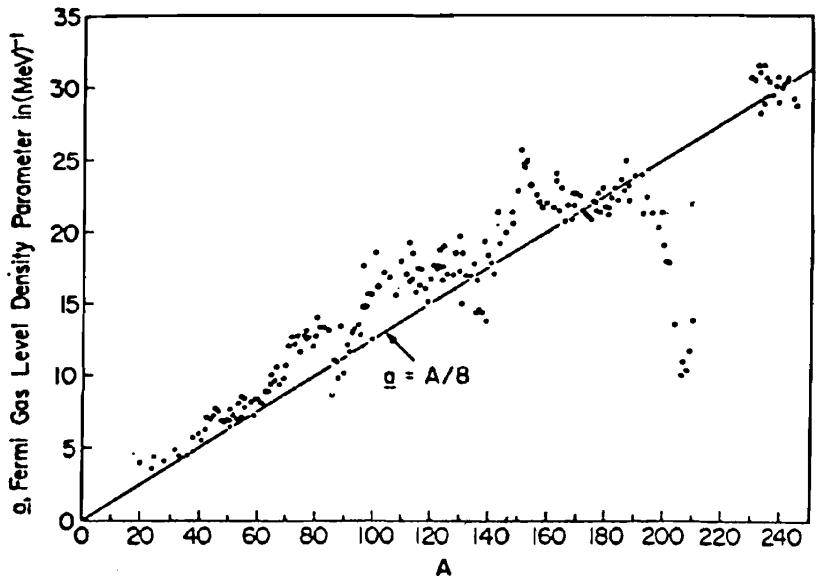

FIG. 4.1. Level density parameter a versus A. The straight line corresponds to $a = A/8$ and dark points are experimental determinations. [From Lefort (76).]

maximum excitation energy for the nucleus, $(E_i + Q_{fi}) \equiv U_M$,

$$\omega_0(E_i + Q_{fi} - E_f) = Ce^{2\sqrt{aU_M}} e^{-E_f/T(U_M)} \tag{4.8}$$

where

$$T(U_M) = \sqrt{\frac{U_M}{a}} \tag{4.9}$$

T is referred to as the *nuclear temperature*,‡ given in energy units. The energy spectrum (4.5) becomes, as far as its dependence on E_f is concerned,

$$\left\langle \frac{d\sigma_{if}}{dE_f} \right\rangle \sim E_f \sigma_c(f; E_f) e^{-E_f/T} \tag{4.10}$$

‡One can obtain a more general formula by postulating

$$\omega_0 = e^{S(U)}$$

Expanding $S(U)$ about U_M yields

$$\omega_0(U) = e^{S(U_M)} e^{-E_f/T} \qquad T^{-1} = \left(\frac{\partial S}{\partial U} \right)_{U = U_M}$$

This formula is similar to that which gives the energy distribution of molecules evaporated from condensed matter. It suggests the picture that the incident particle deposits energy in the system, which then heats to a temperature T and then evaporates. For this reason the low-energy part of the spectrum for which (4.10) is valid is often referred to as the evaporation and/or the *equilibrium region.* An example of the determination of the temperature from experiment is shown in Fig. 4.2.

The angular distribution of the reaction products in the eavaporation region is predicted to be spherical. The derivation of this result employs the assumption that the excitation of the residual nucleus will populate levels with all possible values of and directions of the angular momentum. However, in the case of some systems, particularly those involving the collision of heavy ions, for which large angular momenta are selectively populated, isotropy will no longer be predicted. We shall postpone the discussion of that case to Chapter VIII.

The dependence of the density of levels on angular momentum in the residual nucleus has been derived by Bloch (54) using the independent particle model for the nucleus: The z component of the total angular momentum M (z is in an arbitrary direction) is obtained by adding up the z components of the angular momentum of each of the nucleons making up the residual nucleus. Presuming these components to be random, the probability distribution for a given total $M(\geqslant 0)$ is given by the central limit theorem as

$$F(M) \sim e^{-M(M+1)/2\sigma^2}$$

where σ is the dispersion and $M(M+1)$ rather than M^2 has been put into the exponent. The density of levels with a value of angular momentum equal to I, ω_I, is given by $F(I+1) - F(I)$ since the M component of the angular momentum in the range $(I-1, I)$ must be projected from total angular momenta greater than $I-1$ and less than I. Approximately,

$$F(I-1) - F(I) \sim -\frac{\partial F(I)}{\partial I} dI = \frac{2I+1}{2\sigma^2} e^{-I(I+1)/2\sigma^2} dI \tag{4.11}$$

Hence

$$\omega_I = \frac{(2I+1)\omega_0}{\sqrt{8\pi\sigma^3}} e^{-I(I+1)/2\sigma^2} \tag{4.12}$$

where the the dependence on σ in the coefficient of the exponential has been chosen so that

$$\sum_I \frac{2I+1}{\sqrt{8\pi\sigma^3}} e^{-I(I+1)/2\sigma^2} \approx 1$$

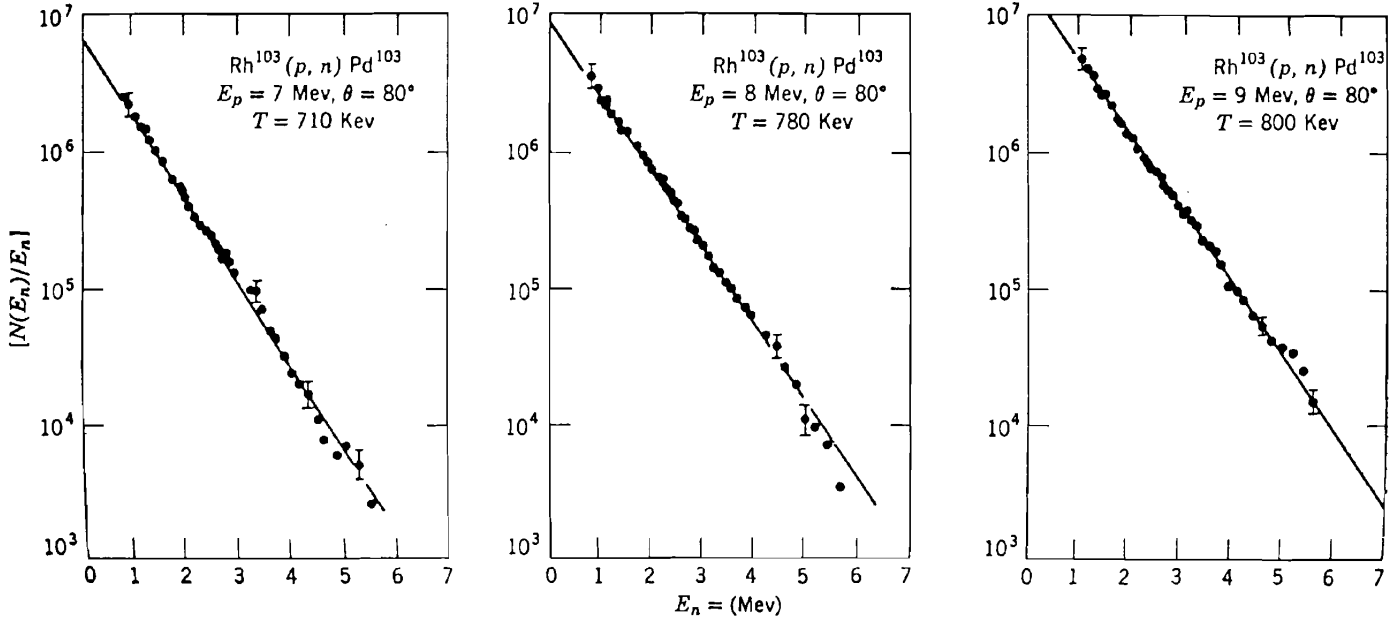

FIG. 4.2. Spectrum of neutrons from the Rh(p, n) reaction at a neutron emission angle of 80°. [From Holbrow and Barschall (63).]

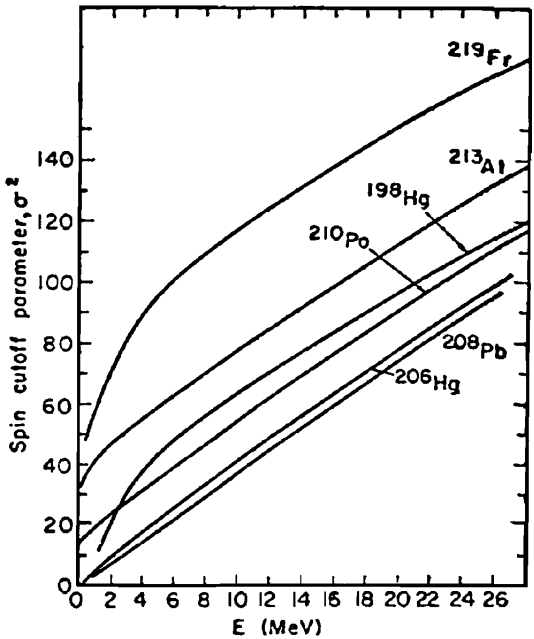

FIG. 4.3. Theoretical spin cutoff parameters σ^2 as a function of excitation energy for nuclei in the ^{208}Pb region (40). The calculations have been performed on the basis of the Nilsson diagram. [From Huizenga and Moretto (72).]

Theoretical values of σ as a function of mass number are shown in Fig. 4.3. Equation (4.5) (for spin-dependent systems) and the isotropy of the reaction products is derived under the assumption that $\omega_I \simeq (2I + 1)\omega_0$, that is, neglecting the exponential in (4.12), an assumption that fails for the collision of heavy ions. This exponential factor expresses the fact that for a given number of nucleons, the number of ways one can construct a total angular momentum, I, from the individual nucleon angular momenta must eventually decrease as I increases.

5. MULTISTEP DIRECT REACTIONS

A wide variety of nuclear reactions cannot be described either as a single-step direct process, that is, by the DWA approximation (4.1), or as a compound nuclear resonance reaction, as extended by the statistical theory of nuclear reactions [see (4.5)]. In terms of Fig. 3.1*b* giving a typical energy spectrum of particles emerging at a given angle (or of the corresponding residual nuclei), the region of validity of these two descriptions is limited to the high-energy region for the direct single-step process, while the statistical compound nuclear process is limited to the low-energy end. The latter domain is characterized by

spherical angular distributions and rapid fluctuations in the energy dependence of the cross section, symptomatic of long interaction times. The direct reaction involves short interaction times and thus is characterized by anisotropic angular distributions and a slowly varying energy dependence of the cross section.

However, in the energy region between high and low energies, large deviations from the predictions of these two mechanisms are found. For example, in Fig. 5.1 the ^{197}Au(α, xn) cross section integrated over angles are compared with the statistical compound theory [see (4.5)] for α-particle energies ranging from 20 to over 70 MeV. Clearly, a rapidly growing discrepancy appears in each of the cross sections shown in the figure.

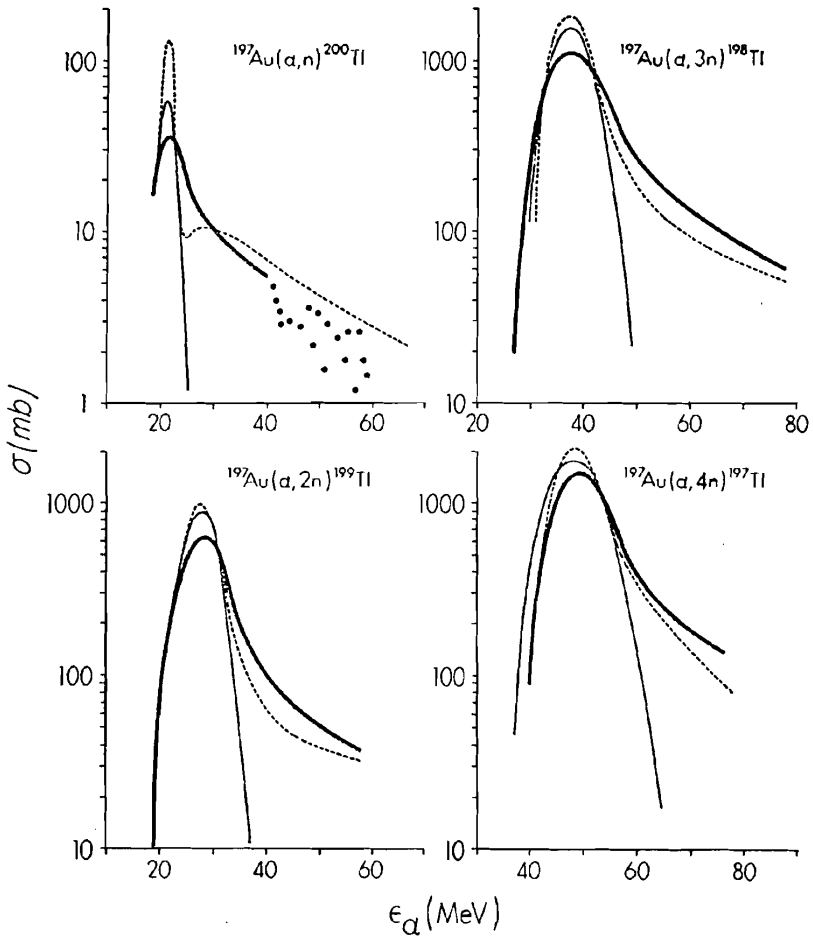

FIG. 5.1. Calculated and experimental excitation functions for the reactions ^{197}Au(α, xn). The heavy solid curves represent experimental yields. The thin solid curves represent equilibrium statistical model calculations. [From Blann (72).]

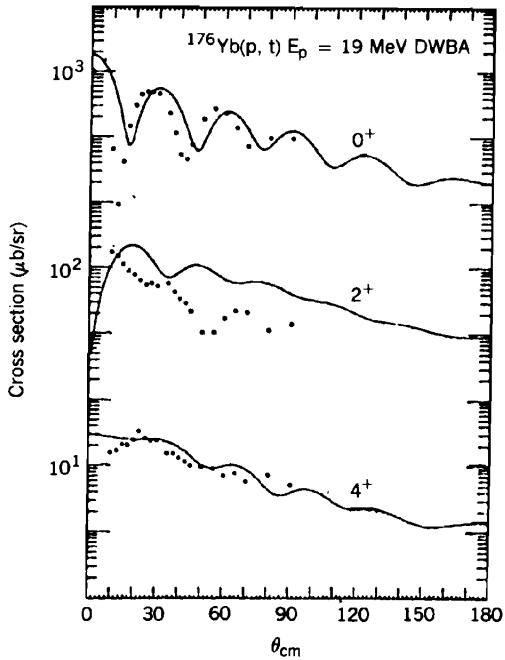

FIG. 5.2. Experimental data for the reaction ^{176}Yb(p, t) compared with the single-step DWA calculation (solid line). [From Ascuitto, Glendenning, and Sørensen (72).]

The single-step direct process can fail to describe reactions at the high-energy end of the spectrum, as illustrated by the reaction ^{176}Yb$(p,t)^{174}$Yb. In Fig. 5.2 the DWA is compared with the experimental result and does not provide an explanation of the angular distribution for the excitation of the 2^+ state by a wide margin.

Both the statistical compound and the direct reaction theories are limiting descriptions, the former involving very long interaction times, the latter, very short reaction times. It is now necessary to retreat from these extremes and consider processes involving intermediate interaction times.

In the case of direct reactions, the procedure to be used is rather obvious. The single-step reaction is described in terms of the DWA. This is a perturbation theory where the perturbing interaction is, according to (4.1), given by $\langle b, Y|V|a, X\rangle$. The amplitude given by (4.1) is an approximation to the more precise amplitude to be obtained from the coupled equations

$$[E_i - T - V_{\text{opt}}(a, X)]\psi(a, X) = \langle a, X|V|b, Y\rangle\psi(b, Y) \tag{5.1a}$$

$$[E_f - T - V_{\text{opt}}(b, Y)]\psi(b, Y) = \langle b, Y|V|a, X\rangle\psi(a, X) \tag{5.1b}$$

where $V_{\text{opt}}(a, X)$ is the optical potential between the target X and projectile a

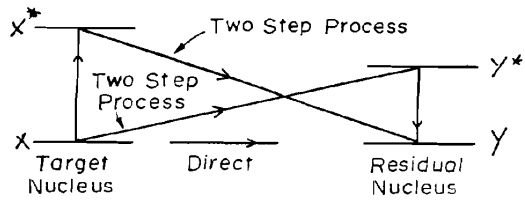

FIG. 5.3

and T is the kinetic energy operator for their relative motion. The amplitude equation (4.1) is obtained by dropping the terms on the right of (5.1*a*).

However, this result still leaves out possibly important physical processes, consequences of the polarizability of the target (residual) nucleus by the projectile (emergent particle). For example, the target nucleus and/or the residual nucleus may be excited, permitting the reaction to the final state to proceed by several intefering routes, as indicated in Fig. 5.3. In addition to the one-step process, there are several two-step amplitudes. In one, the target nucleus is excited and then makes the transition to the final state of the residual nucleus; in another, the transition is from the initial target nucleus to an excited state of the residual nucleus which in the second step of the process is deexcited. In a reaction such as $(^3\mathrm{H}, p)$, in which several nucleons are transferred, interference between the direct route and one in which the nucleons (neutrons in the example) are transferred one at a time is possible. Indeed particle transfer can play a role even in the case of an inelastic scattering (p, p') reaction. It might be the case that the two-step process $X(p, d)Z(d, p')X^*$ is important for some special reason. For example, a collective state (or set of collective states) of nucleus Z might be accessible in the energy, charge, and angular momentum range under investigation.

The two-step process illustrated in Fig. 5.3 is described by the following equations:

$$[E_i - T - V_{\mathrm{opt}}(a,X)]\psi(a,X) = \langle a, X | V | a, X^* \rangle \psi(a, X^*) + \langle a, X | V | b, Y \rangle \psi(b, Y) + \langle a, X | V | b, Y^* \rangle \psi(b, Y^*) \tag{5.2a}$$

$$[E_i - T - \varepsilon_x - V_{\mathrm{opt}}(a, X^*)]\psi(a, X^*) = \langle a, X^* | V | a, X \rangle \psi(a, X) + \langle a, X^* | V | b, Y \rangle \psi(b, Y) \tag{5.2b}$$

FIG. 5.4. (*a*) Cross sections for the 2^+ state that correspond to the individual transfer processes shown. Note that the direct and indirect routes are comparable in magnitude. Each of these overestimate the cross section and interfere destructively to produce the final result. (*b*) Cross sections for members of the ground band of ^{174}Yb. Calculations include all transitions connecting all three states in both nuclei. The 0^+ curve was normalized to the data and the same normalization was used for the other two. [From Ascuitto, Glendenning, and Sørensen (72).]

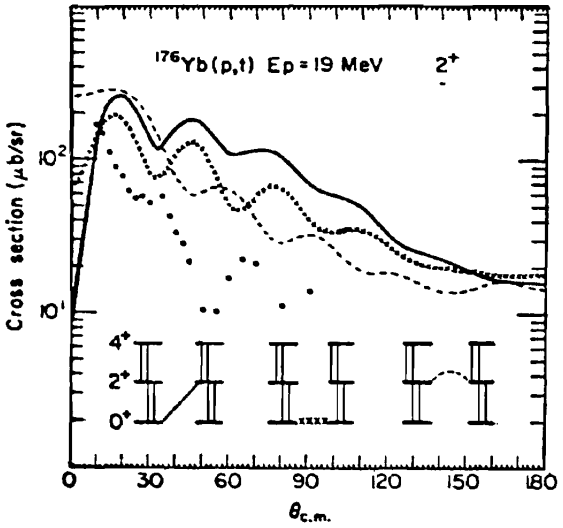
^{176}Yb(p,t) Ep = 19 MeV
2+
Cross section (μb/sr)
10²
10¹
4+
2+
0+
0
30
60
90
120
150
180
θc.m.

(a)

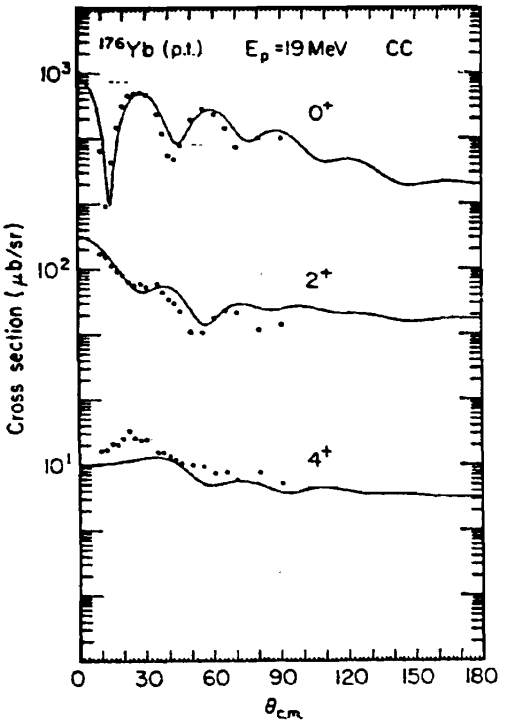
^{176}Yb (p,t) Ep = 19 MeV CC
Cross section (μb/sr)
10³
10²
10¹
0+
2+
4+
0
30
60
90
120
150
180
θcm

(b)

$$[E_f - \varepsilon_y - T - V_{opt}(b, Y^*)]\psi(b, Y^*) = \langle b, Y^* | V | a, X \rangle \psi(a, X) + \langle b, Y^* | V | b, Y \rangle \psi(b, Y) \quad (5.2c)$$

$$[E_f - T - V_{opt}(b, Y)]\psi(b, Y) = \langle b, Y | V | a, X \rangle \psi(a, X) + \langle b, Y | V | a, X^* \rangle \psi(a, X^*) + \langle b, Y | V | b, Y^* \rangle \psi(b, Y^*) \quad (5.2d)$$

The *coupled-channel Born approximation* (CCBA) follows the prescription dictated by the arrows in Fig. 5.3. It is obtained by putting the right-hand side of (5.2*a*) equal to zero, retaining only the terms in $\psi(a, X)$ on the right-hand side of (5.2b) and (5.2c).

Note that the optical potential $V_{opt}(a, X)$ in (5.2*a*) is not identical to the $V_{opt}(a, X)$ of (5.1*a*). The optical potential takes into account, in an average way, the effects of channels that are not explicitly considered. Since these differ for the two cases (5.2*a*) and (5.1*a*), the corresponding $V_{opt}(a, X)$ cannot be equal.

Obviously, the number of coupled equations can be made infinitely large. Practically, what one should do is to take into account the couplings that are felt to be most important for some physical reason; even then there may be a great number of equations. Under these circumstances it often proves more appropriate to use a statistical approach. The statistical theory of multistep direct processes is discussed below.

As an example of the use of multistep processes, consider the reaction discussed earlier, ^{176}Yb$(p, t)^{174}$Yb to the 2^+ state in the residual nucleus. By including the excitations of the ^{176}Yb ground-state band up to 4^+ and the ^{174}Yb ground-state band, we see in Fig. 5.4 that the theoretical predictions now follow the experimental results much more completely than in the single-step DWA theory case. In particular, in the transition routes illustrated in the figure, ground state to ground state with subsequent transition to the 2^+, and excitation of the ground state in the target nucleus to the 2^+ followed by a two-particle transfer to the 2^+ of the residual nucleus, were especially important, as important as the direct excitation.

6. STATISTICAL DOORWAY STATE REACTIONS

We consider now that portion of the spectrum which borders on the low-energy region dominated by the evaporation process. A clue to the mechanism involved is provided by the experiments of Grimes, Anderson, et al. (71) shown in Fig. 6.1. The reaction is ^{59}Co$(p, n)^{59}$Ni. The ordinate is the excitation energy of the residual nucleus ^{59}Ni, so that a large U value corresponds to small neutron energies. As expected from evaporation theory, the lowest-energy neutrons had an isotropic angular distribution. However, as the energy of the neutrons increases, the angular distribution became anisotropic but remained symmetric around 90°. Eventually, this symmetry also disappeared, as indicated on the figure. We pay special attention to the regime in which the angular

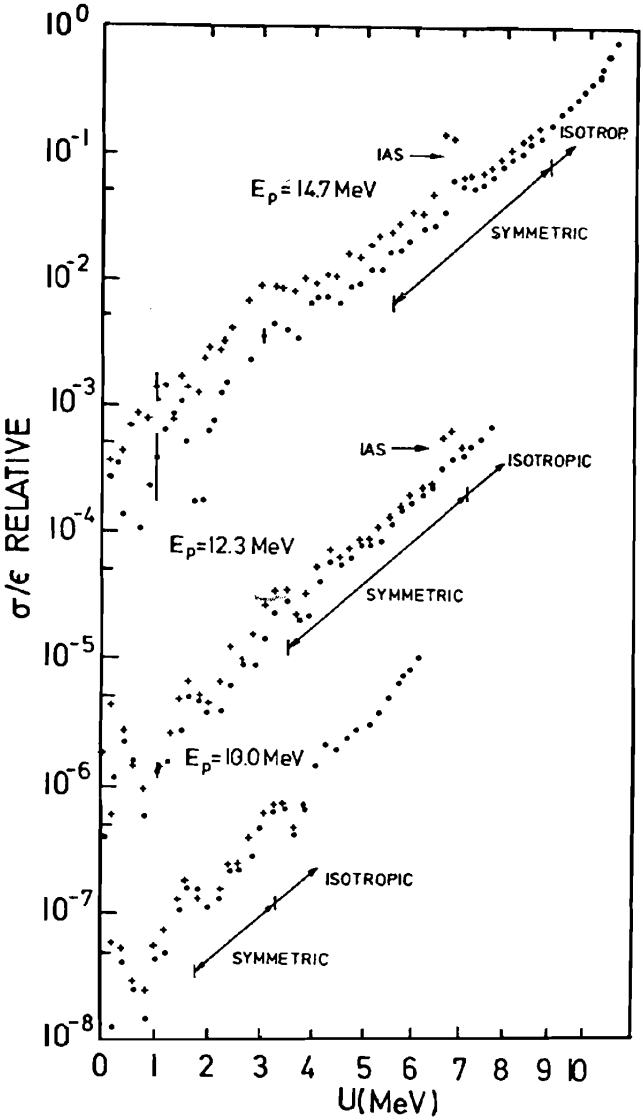

FIG. 6.1. Neutron spectrum for the $^{51}\mathbf{V}(p,n)^{51}$Cr reaction. U is the excitation energy of the residual nucleus. [From Grimes, Anderson, et al. (71).]

distribution is symmetric but no longer isotropic. An examination of all the data reveals that in this excitation region, there are a greater number of higher-energy neutrons than would have been predicted from evaporation theory using the state density Equation (4.7). The symmetry about 90° suggests a statistical mechanism analogous to that discussed in the preceding, section involving compound nuclear resonances, and indeed, Grimes, Anderson, et al.

(71) propose that the resonances now involved are the doorway state resonances. A statistical theory of such doorway state nuclear reactions had been suggested earlier and used explicitly by Block and Feshbach (63).

The concept of the doorway state and the doorway state resonances is described briefly in deShalit and Feshbach (74, pp. 99–104), with particular attention being paid to the isolated doorway state such as the isobar analog state [which by the way, is visible in the data of Grimes, Anderson, et al., (71) shown in Fig. 6.1)]. In the present context, we shall be energy averaging over a number of doorway state resonances, again using the random-phase assumption of Section 4.

The importance of the doorway state in the present context should, in retrospect, not have been surprising. It seems rather obvious tha the interaction time for reactions leading to the domain lying between the low-energy part of the spectrum of Fig. 3.1*b* with its long interaction time and the high-energy end with its short interaction time is intermediate, lying between these two extremes. The intermediate range of interaction times corresponds exactly with the domain in which doorway states should be of importance. As expressed in deShalit and Feshbach (74, p. 99), a cross section can have energy dependence, that is, "structure," which varies (1) over a scale on the order of the compound nuclear width Γ_{CN}, which applies to the evaporation region; (2) over the much broader scale of the single-particle width Γ_{SP}, which applies to the direct reaction region; and (3) over an intermediate scale Γ_d, which is appropriate for the region lying between:

$$\Gamma_{SP} \gg \Gamma_d \gg \Gamma_{CN}$$

The interaction times, τ, vary inversely, so that

$$\tau_{\text{dir}} \ll \tau_d \ll \tau_{\text{EVAP}} \tag{6.1}$$

The dynamical mechanism responsible for the intermediate structure presumes the existence of simple excitations of the system. A simple *example* is shown in Fig. 6.2. The well and the black dots represent schematically the shell

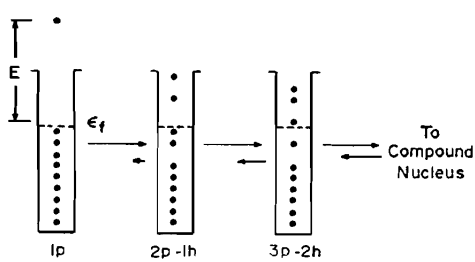

FIG. 6.2. Successive steps in a nuclear reaction leading to the formation of α compound nucleus. [From Blann (73).]

model potential and particle filling levels of that potential, respectively. The incident particle is shown with an incident energy E. It is readily able to excite, via an assumed two-body residual nucleon–nucleon potential, two-particle-one-hole states (2p–1h), which are next in complexity to the incident channel, which in this language is a one-particle (1p) state. The two-body residual potential acting on the $(2p-1h)$ hole states can mix these, can return the system to the simpler 1p state, or can generate (3p–2h) states of still higher complexity. In this way a description of the components of the states of the system in terms of a hierarchy based on increasing complexity can readily be formulated. Obviously, if it is appropriate for the system in question, a model other than the shell model might be used and a different set of definitions would be involved in defining the hierarchy of complexity. It is necessary, perhaps to emphasize that this choise of model is *not* a matter of convenience. It is a statement regarding the nature of the excitations of the system.

To emphasize that point, we replace Fig. 6.2 by Fig. 6.3, in which the set of states next in complexity to the incident channel have been labeled as doorway states and the remaining states have been grouped together in the box entitled "states of higher complexity." The word *doorway* was originally suggested by Block and Feshbach (63) to indicate an additional assumption employed to give the partition of Fig. 6.3 a dynamical significance. That assumption states that with the system starting in the incident channel to excite the states of higher complexity (the third stage in the figure) it is first necessary for the system to involve states of lower complexity, that is, the doorway states. This assumption implies that if the probability of forming doorway states from the incident channel is small, the probability of forming compound nuclear states will be reduced correspondingly. The doorway state assumption can be stated analytically: The matrix elements of the Hamiltonian between the incident channel and the second boxes in Fig. 6.3 are assumed to be zero. This assumption can be justified for the case of the shell model hierarchy classification for a two-body residual interaction. It is not expected that this assumption is obeyed exactly.

We are now ready to exploit the interaction time differences expressed by (6.1). It permits energy averaging over a range ΔE, which is large compared to Γ_{CN} but still small compared to Γ_d, thus preserving the intermediate structure associated with doorway states but smoothing out the fluctuations caused by the compound nuclear state resonances. The average cross section for a doorway state resonance reaction $i \to f$, *omitting the effects of spin and direct reactions*

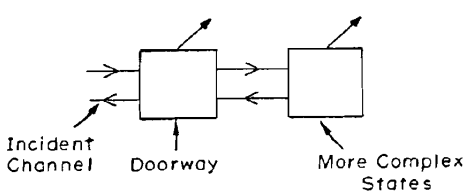

FIG. 6.3

for simplicity is

$$\sigma_{if} = \frac{\pi}{k^2} \frac{\Gamma_{di}^{\uparrow} \Gamma_{df}^{\uparrow}}{(E - E_d)^2 + (\frac{1}{2}\Gamma_d)^2} \tag{6.2}$$

In this formula, $\Gamma_{di}^{\uparrow}$ is the width measuring the probability of forming the doorway state from the incident channel i, while $\Gamma_{df}^{\uparrow}$, the *escape width*, is proportional to the probability that the doorway state will decay into the final channel. Equation (6.2) resembles the expression for the cross section for the same process proceeding through a *compound nuclear resonance*. With the same assumptions as those which apply to (6.2), that cross section is given by

$$\sigma_{if} = \frac{\pi}{k^2} \frac{\Gamma_{\lambda i} \Gamma_{\lambda f}}{(E - E_\lambda)^2 + (\frac{1}{2}\Gamma_\lambda)^2} \tag{6.3}$$

where E_λ is the resonance energy, Γ_λ its width, and $\Gamma_{\lambda a}$ are the partial widths proportional to the probability that a system in the resonant state, denoted by the subscript λ, will decay into channel a. The width of the resonance Γ_λ when the resonance is isolated is related to the partial widths as follows:

$$\Gamma_\lambda = \sum \Gamma_{\lambda a} \tag{6.4}$$

The corresponding relation does not hold for the doorway state width Γ_d. It is not just the sum of $\Gamma_{da}^{\uparrow}$. The physical reason is that the doorway state can decay not only into the open channels but also can make a transition into a more complex state, as indicated by Fig. 6.3, and one must add in the width for this process. Therefore,

$$\Gamma_d = \sum_a \Gamma_{da}^{\uparrow} + \Gamma_d^{\downarrow} \tag{6.5}$$

where $\Gamma_d^{\downarrow}$ is called the *spreading width*.[‡] It is a width that increases the doorway state width because of coupling between the doorway and more complex states. It reflects the fact that the doorway state is not an exact eigenstate of the nuclear Hamiltonian. The compound nuclear resonance would be an exact bound state if all the exit channels were closed. The doorway state would also be an exact bound state if, in addition, the probability of a transition to any more complex state were reduced to zero. In the example of Fig. 6.2, the doorway state becomes an exact bound state composed only of 2p–1h wave functions if the probability of transitions to the simpler 1p state, and to the more complex states such as the 3p–2h states, were zero.

We note that the form of the cross section for a doorway state resonance and that for the compound nuclear resonance are identical. The *only* difference

[‡] Γ_W is used for this width in deShalit and Feshbach (74).

is that exhibited by (6.5): namely, the addition of the spreading width. It is thus possible to use all the results developed for the compound nuclear resonance reaction theory. It is only necessary to bear in mind the "extra" channel, the transition to more complex states, with the width $\Gamma_d^{\downarrow}$. In particular, it is possible to take over the results of the statistical theory of compound nuclear–nuclear reactions [see (4.5)] to obtain for the zero-spin case,

$$\left\langle \frac{d\sigma_{if}}{dE_f} \right\rangle_d = \sigma_d(i, E_i) \frac{k_f^2 \sigma_d(f, E_f)\omega_d(U_{fi})}{\sum_a \int dE_a k_a^2 \sigma_d(a; E_a)\omega_d(U_{ai}) + 2\pi^2 \langle \Gamma_d^{\downarrow} \rangle \omega_d} \tag{6.6}$$

In this expression, σ_d is the cross section for the formation of a doorway state, ω_d the density of doorway states, and $\langle \Gamma_d^{\downarrow} \rangle$ the average spreading width. Although the density of doorway states can be large, it is generally much smaller than the density of compound nuclear states. All the quantities appearing in (6.6) depend on the initial energy and the other quantum numbers for the incident channel, since these features are decisive in determining the nature of the doorway states. The corresponding quantities in (4.5) are not dependent on the initial state since the full complexity of the compound nuclear states is achieved only after many steps beyond the doorway stage, at which stage the memory of the incident situation has become very faint. One important conclusion that can now be drawn is that the Bohr independence hypothesis [see (4.2)] is not valid for the statistical doorway state reactions.

7. STATISTICAL THEORY OF MULTISTEP DIRECT AND MULTISTEP COMPOUND REACTIONS

The system of equations, (5.2) describes a comparatively simple situation. However, as the energy of the projectile increases, the excitations of larger numbers of intermediate states become more probable, with the consequence that the number of coupled equations required for an adequate account of the reaction increases rapidly. One can question the usefulness of solving these even if it were practical and even if the coupling potentials were well known. A more fruitful approach—one that proves to be insightful—asks for statistical quantities (as discussed in Section 4) such as energy-averaged cross sections. Such a theory is referred to as the *statistical theory of multistep direct reactions.*

Similar remarks apply to the generalization of the statistical theory of doorway state reactions. In such a development, the stages beyond the primary doorway stage play an important role and thus must be considered explicitly (see Fig. 7.1). Each stage contains wave functions of a given degree of complexity, as discussed in Section 6. Emission into the reaction channel is possible at each stage, as indicated. The statistical theory of doorway state reactions considers emission only at the doorway stage, while the compound nucleus resonance reaction involves emission far down the chain. With so many steps involved in

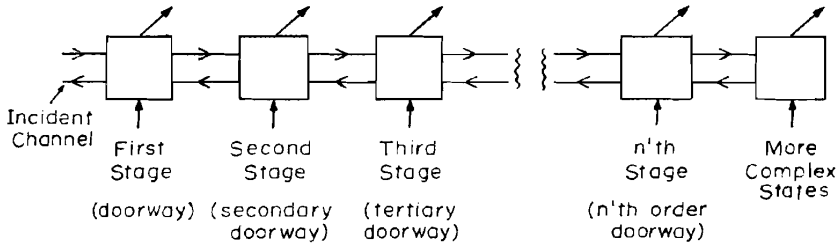

FIG. 7.1

the latter case, it is not surprising that the nature of the initial state is not important for the emission process, thus recovering the Bohr independence hypothesis. Since this chain of stages (Fig. 7.1) can be used to describe the compound nucleus, the reaction type is designated the *multistep compound reaction* to which the adjective "statistical" is added if statistical assumptions are employed in evaluation of the reaction cross sections. As might be expected from the results for the statistical theory of doorway state reactions discussed in Section 6, the statistical theory of multistep compound reactions predicts an angular distribution symmetric about 90°.

This cross section must be added to that obtained for the statistical multistep direct reaction. The latter, with some approximation, can be described as a sequential series of one-step energy-conserving direct reactions. The cross section then consists additively of the contributions from each possible value, n, of the number of steps. However, for a given energy of the emerging particle, there is a most probable value of n, depending on the average energy loss per single-step direct reaction. The angular distribution will generally be anisotropic and asymmetrical. If the angular distribution for the single-step process peaks in the forward direction with the angular width $\delta\theta$, the statistical multistep direct reaction process is predicted to lead again to a forward peak, but the width would now be given by $\sqrt{n}\,\delta\theta$.

8. DIRECT NUCLEAR REACTIONS AND SPECIFICITY

Much of the present-day understanding of nuclear structure, particularly the properties of low-lying states, has been gained from the study of nuclear reactions, particularly the single-step direct type. For this purpose it is necessary to understand the dynamics of nuclear reaction, while at the same time methods must be developed that permit the extraction of nuclear structure information. These two objectives are inextricably involved. Nevertheless, it has proved possible to accomplish both despite the fact that these reactions are governed by the strong interactions. Playing an essential role has been the ability to study the various processes systematically, varying the targets, the projectiles, and projectile energy and exploiting the wide variety of reactions described in Section 3.

The key has been what is termed the *specificity* of, particularly, the direct nuclear reactions [see deShalit and Feshbach (74, p. 72)]. *Specificity* refers to the ability of these nuclear reactions to excite specific types of nuclear states preferentially or to probe particular nuclear properties. Specificity can be a consequence of a property of the projectile, that is, its charge, mass, spin, and so on, and/or it can be a consequence of a property of the initial and final nuclear states connected by the reaction. Generally, specificity can be exhibited for experiments in which specific final states are observed rather than an average over a group of final states appropriate for the statistical models. This requirement calls for precision experiments involving beams and detection equipment with excellent energy resolution. Obviously, observation of particular final states is less easily performed. As the excitation energy increases, the density of levels increases and the energy separation between the levels decreases. By and large this has the consequence that it is in the transition to low-lying states, for which the existence of specificity is most easily observed. This limitation can be violated if a particular reaction mechanism selects out a particular type of state for which the density of states is not very large, even if the excitation energy is high. An example is the excitation of states with a very large angular momentum by heavy-ion projectiles. Another is the excitation of isobar analog states, whose existence is a consequence of the approximate conservation of isospin. Incidentally, the excitation of single states permits the use of conservation principles that help not only to identify the mechanism involved but also to determine the nature of the states excited.

The importance of the single-step direct reaction in this context should be emphasized. As we have described repeatedly, the excitation of complex states will generally require multistep processes. However, multi-step processes do not usually play an important role in the excitation of simple modes of motion.

On the other hand, single-step direct reactions preferentially excite simple modes of motion of nuclei. For example, the stripping (d,p), which adds a neutron to the target nucleus, and the pickup (p,d) reaction, which removes a neutron, are sensitive to the single-particle aspects of nuclei and are thus particularly useful for shell model studies. The added neutron in the first example will be placed in an empty single-particle orbital, producing a particular state of the residual nucleus. The contributions to this cross section from multistep processes will generally be relatively small.

A. Angular Momentum and Coulomb Barriers

Specificity depends on several factors. The one first realized historically is concerned with the probability that a projectile can penetrate to where a nuclear reaction can take place. The most familiar barrier to penetration is the *Coulomb barrier*, present because of the electrostatic repulsion between the positively charged nucleus and the positively charged projectile. This barrier is illustrated in Fig. 8.1. It can be expected that if the energy of the system is well below the peak (see curve A in the figure), the particle will not be able to penetrate and

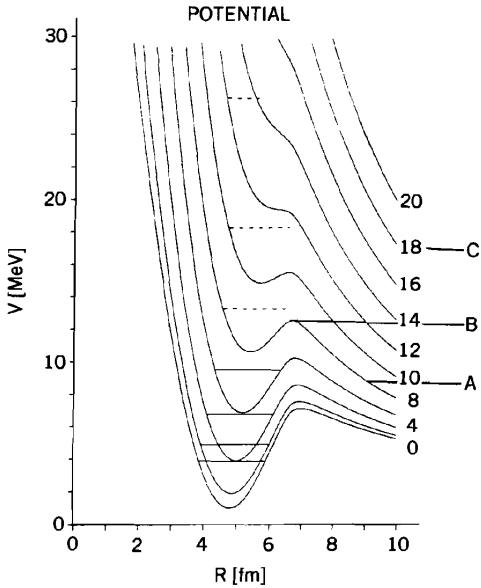

FIG. 8.1. Real potential for $^{12}C-^{12}C$ scattering. [From Scheid, Fink, and Müller (73).]

nuclear reactions will be improbable. On the other hand, when the energy is near the top of the barrier or above (see curves B and C in the figure), penetration will readily be accomplished. The barrier energy is given roughly by

$$E_B = \frac{zZe^2}{R}$$

where ze is the projectile charge, Ze the charge of the target nucleus, and R the distance between the centers of the projectile and target when touching. Replacing R by $1.2(A_T^{1/3} + A_p^{1/3})$ fm, where A_T is the mass number of the target and A_p of the projectile, this formula becomes

$$E_B = 1.22 \frac{zZ}{A_T^{1/3} + A_p^{1/3}} \quad \text{MeV} \tag{8.1}$$

Some representative values are given in Table 8.1.

Another barrier to penetration is the *angular momentum barrier*. Classically, the system, consisting of an incident projectile of momentum p and target nucleus at rest, will have an angular momentum given by pb, where b is the *impact parameter* (see Fig. 8.2). If the *interaction radius*, that is, the distance between the centers of the interacting projectile and target nucleus beyond which nuclear reactions become improbable, is R, the maximum angular

TABLE 8.1

Nucleus	Coulomb Barrier Energy for Protons[a] (MeV)	Coulomb Barrier Energy for α-Particles[a] (MeV)
$^{27}_{13}$Al	3.97	6.96
$^{64}_{29}$Cu	7.07	12.62
$^{108}_{47}$Ag	9.95	18.06
$^{179}_{72}$Hf	13.28	24.30
$^{238}_{93}$U	15.59	28.80

[a]In the radius formula $1.2(A_T^{1/3} + A_p^{1/3})$ the factor 1.2 is determined empirically by charged particle reactions. It can, in fact, be as large as 1.5 in some cases, reducing the values above by the ratio $1.2/1.5 = 0.8$.

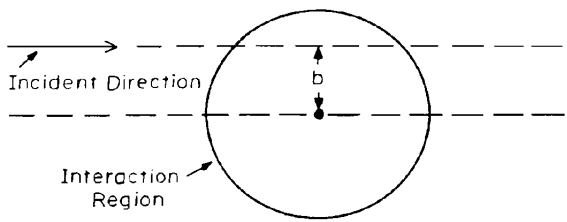

FIG. 8.2

momentum of the system that can contribute to a reaction is pR. Therefore, nuclear reactions will involve angular momenta $l\hbar$, satisfying

$$l \lesssim \frac{pR}{\hbar}$$

$$\lesssim kR \qquad k \equiv \frac{p}{\hbar} \tag{8.2}$$

Numerically (and nonrelativistically) for light projectile.

$$kR = 0.22R(A_pE)^{1/2} \tag{8.3}$$

where R is expressed in fermis, A_p is the projectile mass number, and E is the projectile energy in MeV. For a given energy E the more massive particle carries more angular momentum, so that a heavy-ion projectile is capable of transmitting a relatively larger angular momentum to the target nucleus. In fact, it is in this way (i.e., by heavy-ion collisions) that the very high spin states referred to earlier are excited.

The phrase *angular momentum barrier* emphasizes that kR gives a rough upper bound to the angular momentum which can be involved in a nuclear reaction. Quantum mechanically, the probability for a nuclear reaction falls rapidly but not immediately to zero when the angular momentum kR is exceeded. The angular momentum barrier makes its appearance explicitly as an effective repulsive potential (the centrifugal potential) in the radial Schrödinger equation describing the relative radial motion of projectile and target. The ratio of this centrifugal potential energy to the total energy E evaluated at the interaction radius R is

$$\frac{\hbar^2}{2mE}\frac{l(l+1)}{R^2}$$

which must be less than 1 if the centrifugal barrier is to be penetrated easily. On introducing the variable k, this condition becomes

$$l(l+1) \lesssim (kR)^2 \tag{8.4}$$

which is just the quantum-mechanical equivalent of (8.2).

Roughly, the probability for a nuclear interaction is proportional to the probability that the incident particle will arrive at the nuclear surface. For neutral particles such as the neutron, the incident amplitude for a wave carrying angular momentum $l\hbar$ is proportional to the spherical Bessel function of order $l, j_l(k_i r)$, where k_i is the incident momentum divided by $\hbar$. The corresponding probability evaluated at the nuclear radius R is $j_l^2(k_i R)$, which for small $k_i R$ is on the order of $(k_i R)^{2l}$. The fact that this quantity approaches zero for small k_i is simply the expression of inequality (8.4).

The effect of the Coulomb barrier is given for small values of $k_i R$ by multiplying the neutral penetration factor by one depending on the dimensionless parameter η_i:

$$\eta_i = \frac{zZe^2}{\hbar v_i} = \frac{E_B R}{\hbar v_i} \tag{8.5}$$

where ze is the projectile charge, Ze the target nucleus charge, and v_i the incident velocity. One obtains for the penetration factor

$$C_l^2(\eta_i)(k_i R)^{2l}$$

where

$$C_l^2 = \frac{2^{2l}}{[\Gamma(2l+1)]^2}[l^2+\eta_i^2][(l-1)^2+\eta_i^2]\cdots[1+\eta_i^2]\frac{2\pi\eta_i}{e^{2\pi\eta_i}-1} \tag{8.6}$$

The last factor is the value of C_l^2 for $l=0$, C_0^2. This factor goes to zero rapidly

TABLE 8.2

η	$C_0^2(\eta)$
0	1.000
0.2	0.500
0.4	0.222
0.6	0.089
0.8	0.033
1.0	1.18×10^{-2}
2.0	4.38×10^{-5}

as the barrier energy increases or as the incident velocity decreases, as can be seen from Table 8.2, indicating the strong effect of the Coulomb repulsion. Similar factors $(k_f R)^{2l}$ and $C_l^2(\eta_f)(k_f R)^{2l}$ are present in the cross section for endoergic reactions, for which the emergent particle's momentum can approach zero.

B. Inside the Nucleus

Finally, we come to the question of how far a projectile will travel inside the nucleus once it penetrates the barrier. More precisely, how soon will the incident projectile leave the incident channel, that is, the elastic scattering channel? Empirical evidence indicates that the absorption of neutrons and protons in the nuclear interior is weak. It is, however, very strong for composite systems such as deuterons, α-particles, or heavy ions because these "dissolve" inside the nuclear interior and do not preserve their identity. Thus the composite particles do not penetrate a great distance into the nucleus and tend to be more sensitive to surface properties of nuclei and to excite surface states. The proton does not show such selectivity since it can penetrate the nuclear interior. This is illustrated in Fig. I.10.3 in deShalit and Feshbach (74), where one sees a marked difference in the number of levels excited in inelastic proton scattering compared to inelastic deuteron scattering. In the latter case one would expect a preference for the excitations of the vibrational modes of a nucleus [see deShalit and Feshbach (74, p. 471)].

Let us illustrate these remarks with simple examples. Neutrons and γ-rays are uncharged and thus do not have to penetrate the Coulomb barrier. Neutrons of low kinetic energy are thus the appropriate projectiles to be employed for the study of these states of the *compound nucleus*, formed by the neutron and target nucleus, whose excitation energy is near the separation energy of the neutron. It is in this region that an enormous number of compound nuclear resonances have been found. These are nearly bound states of the compound nucleus. [see Figs. I.12.2 and I.12.3 in deShalit and Feshbach (74); note the neutron energies.]

At very low energies, these resonances must, according to (8.4), be $l = 0$ resonances. As the energy increases, it becomes possible to excite $l = 1$ resonances

and at higher energies $l = 2$ resonances, and so on. For example, for the target nucleus, ^{64}Cu, kR is $\sqrt{2}$ for 1.8 MeV neutrons. It equals $\sqrt{6}$, appropriate for the $l = 2$ case for 5.4 MeV. Of course, both $l = 1$ and $l = 2$ resonances will make their appearance long before these values are reached. Their presence can be demonstrated by, for example, examining the angular distributions of elastically scattered neutrons at and near the resonant energy.

γ-Rays may be used to excite the target nucleus by absorption and in principle could be used to study any of the nuclear states. However, the angular momentum barrier plays a role. If a photon of energy $\hbar\omega$ is absorbed at a distance R from the center of the nucleus, it can transmit an angular momentum of $\hbar\omega R/c$, so that

$$l \lesssim \frac{\hbar\omega R}{\hbar c} = kR \qquad k \equiv \frac{\omega}{c}$$

Since $\hbar c = 197.32$ MeV fm, it is clear that for photon energies up to the order of a few tens of MeV, the photon absorption process will be dominated by the $l = 1$ (i.e., dipole) mode. Quadrupole and higher multipoles will also be absorbed, but the cross sections will be considerably smaller. This effect is clearly visible in the long-wavelength limit. In that limit the transition probability [see (VIII.5.35) deShalit and Feshbach (74)] is proportional to $(kR)^{2j+1}$, where j is the multipole order, so that the transition probability decreases rapidly with increasing j. It is, of course, no accident that the most readily observable gamma-induced reaction, the giant resonance seen in all nuclei [see pp. 48 and 491–503 in deShalit and Feshbach (74)], is a dipole resonance.

A major problem with the use of uncharged particles is the difficulty to measure and control them. The use of lithium-drifted germanium counters has vastly improved the detection of γ-rays, while in recent years the development of nano- and picosecond circuitry, together with the availability of more intense neutron sources, has changed the situation in neutron physics with regard to, for example, the study of (n, n'), (n, γ), and $(n, n'X)$ reactions.

C. Electron Excitation

Since electrons are negatively charged, they are attracted by the positively charged target nucleus. The importance of elastic electron scattering for determination of the nuclear charge density has been emphasized in deShalit and Feshbach (74, pp. 3–7). Here the excitation of nuclear levels by electrons is discussed briefly. We shall consider *only* the effect of the Coulomb interaction:

$$V = \sum_{\text{prot}} \frac{e^2}{|\mathbf{r} - \mathbf{r}_i|} \tag{8.7}$$

where the sum is taken over all the protons in the nucleus and $\mathbf{r}$ is the electron

coordinate. There are other terms involving the magnetic-type interaction and the interaction with exchange currents.

It is, of course, one of the great advantages of using the electron as a probe that the interaction is well known. In addition, the interaction is relatively weak, so that one can use the Born approximation.‡ For simplicity, we shall use the nonrelativistic form, which is incorrect for the high-energy electrons used. However, to some extent, it will be possible to correct for this error in the course of the calculation. The Born approximation inelastic amplitude is

$$f_{fi} = -\frac{1}{4\pi}\frac{2m}{\hbar^2}\int\cdots\int e^{-i\mathbf{k}_f\cdot\mathbf{r}}\Phi_f^*(1,2,\ldots,A)\sum_{\text{prot}}\frac{e^2}{|\mathbf{r}-\mathbf{r}_i|}\Phi_i(1,2,\ldots,A) \times e^{i\mathbf{k}_i\cdot\mathbf{r}}\,d\mathbf{r}\,d(1)\cdots d(A-1) \tag{8.8}$$

or

$$f_{fi} = -\frac{1}{4\pi}\frac{2m}{\hbar^2}\sum_{\text{prot}}\int e^{-i\mathbf{k}_f\cdot(\mathbf{r}-\mathbf{r}_i)}e^{i\mathbf{k}_i\cdot(\mathbf{r}-\mathbf{r}_i)}\frac{l^2}{|\mathbf{r}-\mathbf{r}_i|}d\mathbf{r}\int\cdots\int e^{-i\mathbf{k}_f\cdot\mathbf{r}_i}e^{i\mathbf{k}_i\cdot\mathbf{r}_i} \times \Phi_f^*(1,2,\ldots,A)\Phi_i(1,2,\ldots,A)\,d(1)\cdots d(A-1)$$

where Φ_f and Φ_i are the final and initial states of the nucleus, respectively. Since all the particles are idential, each of the terms in the sum is numerically identical. Therefore, with a change of variable,

$$f_{fi} = -\frac{1}{4\pi}\frac{2m}{\hbar^2}\int e^{i\mathbf{q}\cdot\boldsymbol{\xi}}\frac{Ze^2}{\xi}d\boldsymbol{\xi}\langle\Phi_f|e^{i\mathbf{q}\cdot\mathbf{r}_1}|\Phi_i\rangle$$

where

$$\mathbf{q} = \mathbf{k}_i - \mathbf{k}_f \tag{8.9}$$

and $\mathbf{r}_1$ is the coordinate of one of the protons in the target nucleus. The first factor is the nonrelativistic Born approximation for the elastic scattering of an electron by a point nucleus of charge Ze. We shall replace it by the exact relativistic elastic scattering amplitude. Hence

$$f_{fi} = f_c(\mathbf{q})\bar{\rho}_{fi}^{(c)}(\mathbf{q}) \tag{8.10}$$

where $\bar{\rho}_{fi}^{(c)}$ is

$$\bar{\rho}_{fi}^{(c)} \equiv \langle\Phi_f|e^{i\mathbf{q}\cdot\mathbf{r}_1}|\Phi_i\rangle$$

‡For nuclei with large Z one must take the Coulomb distortion of the electron wave function into account. This will, however, not change the qualitative nature of the results obtained here.

$\bar{\rho}_{fi}^{(c)}(\mathbf{q})$ is the *form factor* for the transition. It is the Fourier transform of the transition charge density

$$\rho_{fi}^{(c)}(\mathbf{r}_1) = \int d(2)\cdots d(A-1)\Phi_f^*(1,2,\ldots,A)\Phi_i(1,2,\ldots,A) \tag{8.11}$$

and

$$\bar{\rho}_{fi}^{(c)}(\mathbf{q}) = \int e^{i\mathbf{q}\cdot\mathbf{r}_1}\rho_{fi}^{(c)}(\mathbf{r}_1)\,d\mathbf{r}_1 \tag{8.12}$$

It is the last quantity that is determined by experiment.

The transition will involve an angular momentum change of j and thus those components of $e^{i\mathbf{q}\cdot\mathbf{r}_1}$ that carry at least that amount of angular momentum will

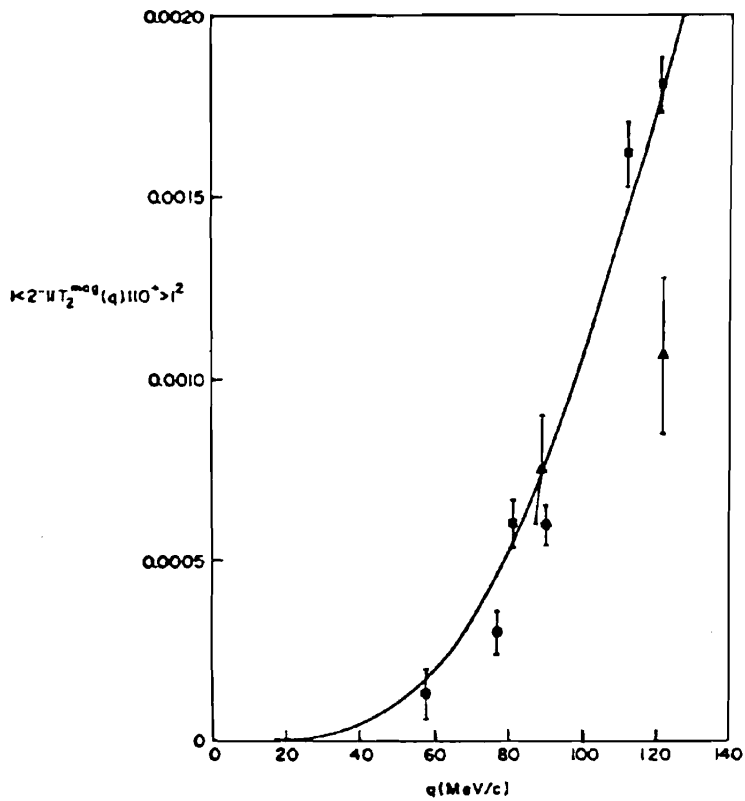

FIG. 8.3. Square of the magnetic form factor for the 2^-, $T=1$ state at 20.76 MeV in ^{12}C. The theoretical calculation divided by 2 is compared with experiment. [From deForest and Walecka (66).]

survive the integration, that is

$$\bar{\rho}_{fi}^{(c)}(\mathbf{q}) = \sum_{l \geqslant j} (2l+1) i^l \int j_l(qr_1) P_l(\cos \vartheta_1) \rho_{fi}^{(c)}(\mathbf{r}_1)\, d\mathbf{r}_1$$

For not too large q, the first term in this sum dominates:

$$\bar{\rho}_{fi}^{(c)}(\mathbf{q}) \sim (2j+1) i^j \int j_j(qr_1) P_j(\cos \vartheta_1) \rho_{fi}^{(c)}(\mathbf{r}_1)\, d\mathbf{r}_1 \tag{8.13}$$

$$\sim \frac{i^j q^j}{(2j-1)!!} \int r_1^j P_j(\cos \vartheta_1) \rho_{fi}^{(c)}(\mathbf{r}_1)\, d\mathbf{r}_1 \tag{8.14}$$

The integral gives the *transition electric multipole moment*. The characteristic dependence on q^j of (8.14) is a reflection of the angular momentum barrier penetration. However, in contrast with the radiative case, for which q is limited to ω/c, where $\hbar\omega$ is the excitation energy, q in the electron inelastic scattering case can be varied from the minimum value of ω/c to a maximum available at back angles given by $(k_f + k_i) \approx 2E/\hbar c$, where E is the electron energy. It thus is possible to use inelastic electron scattering to map out $\bar{\rho}_{fi}^{(c)}(q)$ over a wide range in q, and therefore $\rho_{fi}^{(c)}(r)$, the γ-ray-induced transition providing only $\bar{\rho}_{fi}^{(c)}(\sim 0)$. It should be noted that the dependence q^j helps to identify the multipole moment (but not its electric or magnetic nature), as illustrated by Fig. 8.3.

D. Coulomb Excitation

As implied by the term *barrier*, the Coulomb and angular momentum barriers generally reduce the probability of a nuclear reaction as demonstrated by (8.4) and (8.6). However, this assumes that the reactions are induced by short-range forces. This assumption fails for the Coulomb force. A heavy ion of moderate energy passing at some distance from the target nucleus can still excite the nucleus through the action of the Coulomb force. This mechanism is referred to as *Coulomb excitation*. It is more effective the larger the atomic number of the heavy-ion projectile. By proper choice of the projectile and energy, one can adjust the distance of closest approach so that the projectile does not come too close to the nucleus, so that whatever excitation is observed is caused by the changing electric field associated with the motion of the projectile. Coulomb excitation will preferentially excite levels that have a high probability for γ-emission and indeed has been the method of choice for investigating the rotational spectrum of deformed nuclei [see deShalit and Feshbach (74, p. 412)]. A rough estimate of the Coulomb excitation cross section can be obtained using the Weizsäcker–Williams approximation. This approximation, which becomes increasingly valid as the projectile energy increases, replaces an incident charged

projectile by an equivalent beam of photons with a spectrum given by

$$dn(\omega) = \frac{2}{\pi}\frac{Ze^2}{\hbar v}\frac{d\omega}{\omega} \tag{8.15}$$

where v is the velocity of the projectile. The cross section is then given by multiplying this spectrum by the cross section for the absorption of a γ-ray of energy $\hbar\omega$. Using (VIII.(8.1)) from deShalit and Feshbach (74), assuming zero width for the excited state, one obtains the following for the excitation cross section:

$$\sigma = (4\pi)^2 \frac{Ze^2}{\hbar v}\frac{e^2}{\hbar c}\frac{j+1}{j(2j+1)[(2j+1)!!]^2}k^{2j-2}B(\sigma_j; i \to f) \tag{8.16}$$

This formula should be considered of qualitative validity only in view of the shortcomings of the Weiszäcker–Williams approximation in the energy range in question. It does show the direct connection of the Coulomb excitation cross section with the B coefficients.

The Coulomb field exerted by a heavy ion is very strong. Evaluating the field of a heavy ion of charge z at the target nuclear radius R_T, one finds that the force F on a target nucleus, mass number A_T, and charge Ze is

$$F = \frac{zZe^2}{R_T^2} \simeq \frac{zZ}{A_T^{2/3}} \qquad \text{MeV/fm} \tag{8.17}$$

For a ^{64}Cu projectile incident on ^{208}Pb, $F = 68$ MeV/fm. Such a strong force permits multiple excitations; that is, the target nucleus while excited can be excited once more and the process can be repeated during the course of the collision. This means that the target nucleus will be in one of this chain of possible excited states for a finite time, with the consequence that the properties of such a state can be investigated. In this way the quadrupole moments of excited states have been measured.

E. Surface Reactions

As we stated earlier, composite particle projectiles do not penetrate the target because of absorption. These reactions thus probe the surface of the nucleus. The fact that only the surface is involed means that the important incident angular momenta are in the neighborhood of p_iR, where p_i is the initial momentum of the projectile, while the angular momentum carried off by the emerging projectile is p_fR, where p_f is the final momentum. Hence it will be most probable to excite the target to a level whose angular momentum differs from the ground state by qR, where $q = |\mathbf{p}_i - \mathbf{p}_f|$. This implies a maximum in

the angular distribution at an angle determined by

$$\hbar\Delta J = qR$$

or

$$1 - \cos\theta_M = \frac{(\hbar\Delta J/R)^2 - (p_i - p_f)^2}{2p_i p_f} \tag{8.18}$$

This angle becomes larger as the angular momentum change ΔJ increases. Since, classically, qR must be larger than $\hbar\Delta J$, the cross section is zero classically for $qR < \hbar\Delta J$. This phenomenon is illustrated in Fig. I.11.2b of deShalit and Feshbach (74), in which the angular distribution for the inelastic excitation of various levels in ^{58}Ni by α-particles is shown. One sees that the first peak (excluding a possible peak at 0°) occurs at greater angles as l, the angular momentum of the levels, increases. The angles θ_M predicted from (8.18) are 6.2°, 9.2°, and 12.1°, which compare with 10°, 15°, and 17° experimentally. One also observes a drop in the cross section as one decreases the angle for the $l = 3$ and 4 cases.

The angles predicted from (8.18) are not quite correct since the reduction in momentum that occurs because of the Coulomb repulsion was not taken into account. The Coulomb reduced momentum, p_c, is related to the momentum p (either the incident or final momentum) by

$$p_c = p\left(1 - \frac{zZe^2}{ER}\right)^{1/2} \tag{8.19}$$

where E is the energy. Then using $(p_c)_i$ and $(p_c)_f$ in (8.18) instead of p_i and p_f gives values of θ_M equal to 10.4°, 15.5°, and 20.3°, which compare more favourably with the experimental values. Of course, these simple predictions are substantially modified by quantum-mechanical effects as well as by the effects of the interaction with the target.

An indication of the narrow range in orbital angular momenta involved in reactions of this type is shown in Fig. 8.4. In this case of α-particle inelastic scattering by ^{24}Mg at $E = 84$ MeV, the behavior of imaginary parts of the radial integrals involved in the calculation of the cross section for the process is plotted as a function of the average $\bar{l} = (l_i + l_f)/2$, where l_i is the angular momentum of the incident wave and l_f of the emergent wave. We see that most of the radial integral is concentrated in the region $\bar{l} = 18 \pm 2$. This is in reasonably close agreement wth pR/$\hbar$, which for the R of 3.841 fm used in these calculations equals 15.2. One also notes a very strong oscillation in the angular distribution (see Fig. 8.5). This is the case because the reaction occurs only at the surface, with the consequence that the α-particle is diffracted by the target. Typically, the angular distribution is proportional to $[j_l(qR)]^2$ (j_l is the spherical Bessel

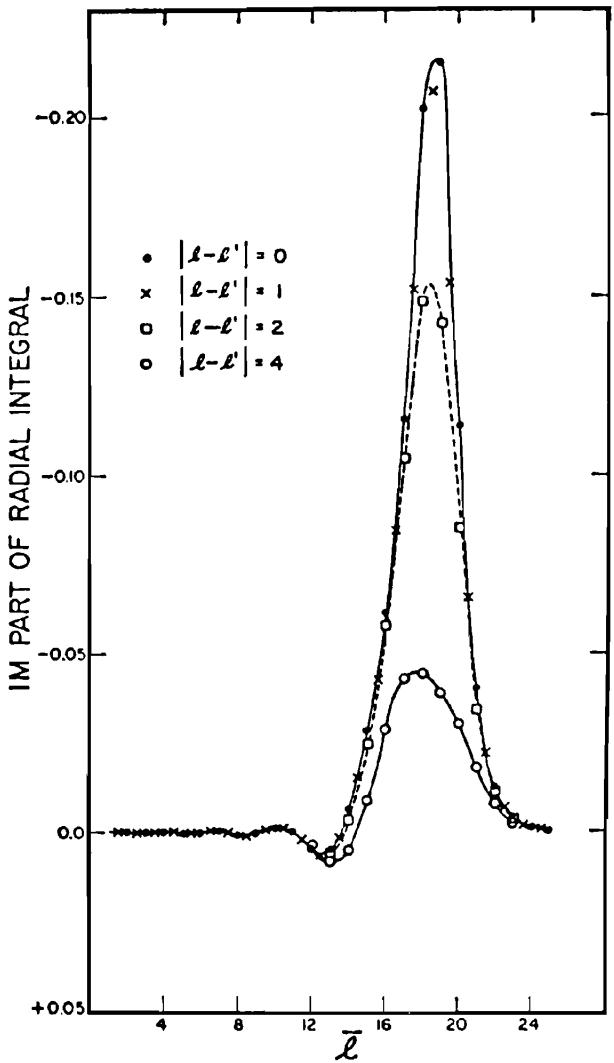

FIG. 8.4. Localization of the radial integrals for $Mg^{24}(\alpha, \alpha')$. [From Austern (70).]

function; see Appendix A). Indeed, as pointed out in Chapter I of deShalit and Feshbach (74, p. 79), this phenomenon can be used to determine R, the effective radius for the reaction being studied.

F. Stripping and Pickup

As discussed earlier, the stripping and pickup reactions result in the deposition (stripping) or removal of a neutron (pickup) from a single-particle orbit. Since

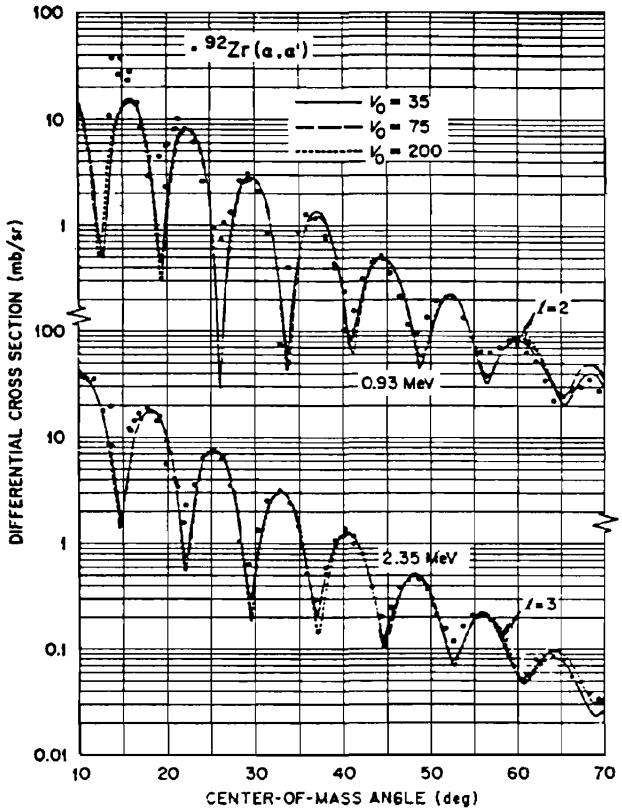

FIG. 8.5. Comparison of the DWA theory with experimental data for $Zr^{92}(\alpha, \alpha')$ at 65 MeV bombarding energy. The energies and angular momenta of the Z^{92} excited states are given on the graph. [From Austern (70).]

the deuteron is strongly absorbed, the cross section will be largest if the single-particle wave-function is appreciable at the nuclear surface. For this reason the valence neutrons are generally involved. For example, in the $^{40}Ca(d, p)^{41}Ca$ reaction of Fig. I.12.1 in deShalit and Feshbach (74), the neutron can go into the $1f_{7/2}$ orbit or higher orbits. However, the state in ^{41}Ca that is excited is generally not pure $\phi(f_{7/2})\Psi_T(^{40}Ca)$ but will have other components. As a consequence, before comparison with experiment is possible, the magnitude of the cross section calculated using (4.1) must be multiplied by a factor, the *spectroscopic factor*, less than unity. The spectroscopic factor gives the probability of finding the final system in the state $\phi(f_{7/2})\Psi_T(^{40}Ca)$. One of the results of the measurement is the energy of the state in question, so that one can map out the energy of the single-particle (or quasi-single-particle) states for a large variety of nuclei. The results are shown in Fig. 8.6.

Neutrons are also added to or removed from a target nucleus by the (n, γ)

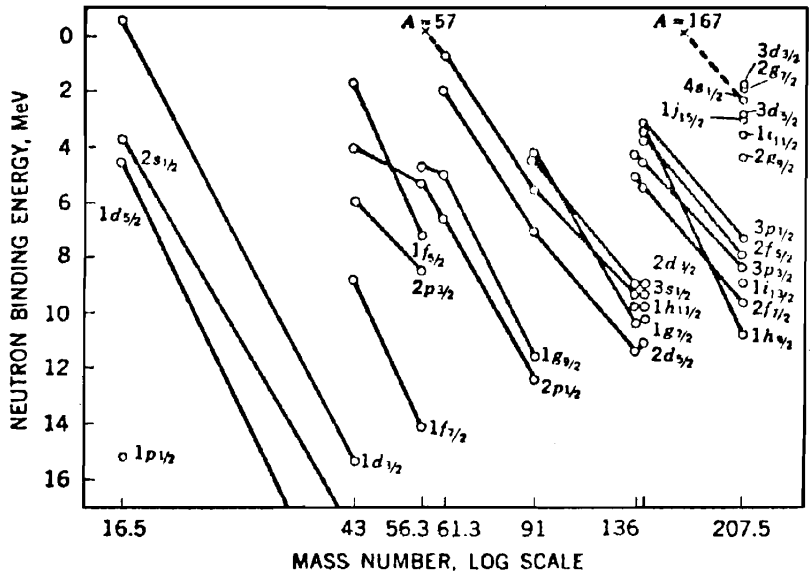

FIG. 8.6. Energies of neutron orbits in various single-particle and single-hole nuclei. Small corrections for symmetry energy have been applied to correct the data to the line of beta stability. [From Cohen (71).]

and (γ, n) processes, respectively. By choosing the appropriate γ-ray energy, one can select some of the states populated by (d, p) or (p, d) reactions. The comparison between the two sets of reaction is informative both as to the nature of the reactions and the states excited. The neutron absorbed is usually a low-energy neutron limiting the angular momentum of the quantum numbers of the compound nucleus. The (γ, n) reaction, on the other hand, is not limited to the removal of neutrons in surface orbitals as is the (p, d) reaction.

The pickup process, (p, d), may be discussed in similar terms. The neutron that is "picked up" is, for the following reason, again a surface neutron in the sense that its wave function peaks at the surface. If the deuteron is made too deeply within the nuclear interior, it will be absorbed before it can escape from the nucleus. Hence surface production will be more visible.

As the energy increases the deuteron will eventually have a large enough mean free path that its production in the interior of the nucleus will be observable. In that case the state of the residual nucleus will, in shell model terminology, be a hole state.[‡] Observations of such states by this method have been made. We mentioned earlier another method of observing single hole states by the (γ, n) reaction and by quasi-elastic scattering of energetic electrons or protons

[‡]The reader should recall that the definition of a hole state depends on the "vacuum" chosen. For example, the removal of a neutron from ^{18}O could be described as leaving a hole state in ^{18}O or leaving a 2p–1h state with an ^{16}O core.

in the $(e, e'p)$ or $(p, 2p)$ reaction, respectively. A comparison of the results obtained with these various methods will provide information on the reaction mechanisms involved as well as the nature of the excited state.

For the stripping and pickup processes, it is important to realize that the single-particle or single-hole states that are probed are surface states not only in configuration space but also in momentum space; that is, for the most part we are dealing with states near the Fermi momentum p_F. Much the same can be said of the excitations induced by other composite particles. The vibrations seen with inelastic α-particles are, for the most part, coherent linear combinations of one-particle-one-hole states, but the major contributions come from states close to p_F.

G. Examples of Direct Reactions

The stripping and pickup reactions are archetypes of the use of direct reaction to study nuclear structure. By choosing the appropriate projectile and energy, it becomes possible to study a wide variety of nuclei and excitations. We earlier mentioned the use of the $(^3\text{He}, d)$ and $(d, ^3\text{He})$ reactions to study single-particle proton states and the $(^3\text{H}, p)$ and $(p, ^3\text{H})$ to study "superconducting" nuclei by the transfer of two neutrons coupled in a $^1S_0$ state. Inelastic proton and neutron scattering will study the formation of 1p–1h states.‡

H. Heavy Ions

The availability of heavy ions greatly increases the variety of projectiles and the range of possible transfers of particles from and to the heavy ions and the target nuclei. The transfer of α-particles is conveniently studied using ^{6}Li projectiles, for example. The nuclei ^{17}O and ^{18}O are useful projectiles for the study of single- and two-neutron transfers. Heavier nuclei are neutron rich and thus facilitate the transfer of many neutrons and the consequent formation of new nuclei approaching more closely those nuclei that are unstable against neutron emission. On the other hand, the same process can lead to the formation of multiparticle–hole states.

In the case of heavy-ion projectiles, it is often the case that the single-step direct description is inadequate and one must turn to the multistep direct processes. Virtual excitation of the low-lying levels in both the projectile and target nucleus can play a role. The sequential transfer of nucleons, resulting in

‡We repeat a caveat. The independent-particle model description of nuclei is oversimplified. The ground state of ^{16}O, for example, consists of the independent-particle state marking the completion of the *p*-shell but also 2p–2h and 4p–4h components, to mention the most likely. These are essential for proper descriptions of the correlations in the ground state. It is convenient to adopt the terminology of Chapter VII in deShalit and Feshbach (74) and refer to the more complete description of single-particle states as *quasi-single-particle* states and the states obtained by inelastic excitation as *quasi-particle-hole* states.

a many-nucleon transfer, can compete with the transfer of the entire cluster as a single-step process.

Because heavy ions are composite, they generally do not penetrate deeply into the target nucleus. Most of the transfer reactions discussed above occur close to the nuclear surface, and thus the heavy ions serve as probes of the surface. The effectiveness of heavy ions in this respect is accentuated by their very short wavelength, which is given by

$$\lambda\!\!\!^{-} = \frac{4.56}{(AE)^{1/2}} \quad \text{fm} \tag{8.20}$$

where A is the projectile mass, E its energy in MeV, and $\lambda\!\!\!^{-}$ is in fermis. For example, if an electrostatic accelerator of the van de Graaf type has an effective terminal voltage of 20 MV, a ^{32}S ion stripped of half its electrons will acquire an energy of 5 MeV per nucleon. Under these circumstances $\lambda\!\!\!^{-}$ equals 6.4×10^{-15} cm! This very short wavelength permits the use of classical mechanics for the discussion of the motion of a heavy ion. Second, it demonstrates the possibility of using a heavy ion as a probe of the surface structure of the target with considerable spatial resolution.

An example of the discussion above is provided by the interaction of ^{16}O ions with ^{60}Ni. The angular distribution, shown in Fig. 8.7, shows rapid oscillations at small angles. This effect can be understood by examining the classical orbits of the ^{16}O ion in the field of the ^{160}Ni nucleus taking the nuclear interaction as well as the Coulomb interaction into account (see Fig. 8.8). It will be observed that orbit 1 above the grazing orbit, g, and orbit 3 give rise to identical scattering angles; in the latter case the nuclear interaction plays an essential role. However, it might be expected that orbit 3 would not be of much importance because of the absorption that takes place in passing through the surface region of the target nucleus. To explain the observations, this expectation must be incorrect. In the surface region involved in the small-angle scattering (and one can be quite specific about that region because of the short wavelength involved), the absorption must be weak, an important conclusion that so far seems to be valid for a variety of heavy-ion reactions.

The procedure employed to obtain the foregoing conclusion is of general interest. It is familiar from *physical optics*, where characteristically the wavelength of light is very much smaller than the dimensions of the components of the optical system. In physical optics the motion of the incident plane wave is "broken up" into the behavior of rays, which is calculated by the methods of classical mechanics. Each ray follows the classical orbit illustrated in Fig. 8.8. The phase of the wave along each ray is obtained by calculating the optical path length given by

$$\int n\, ds$$

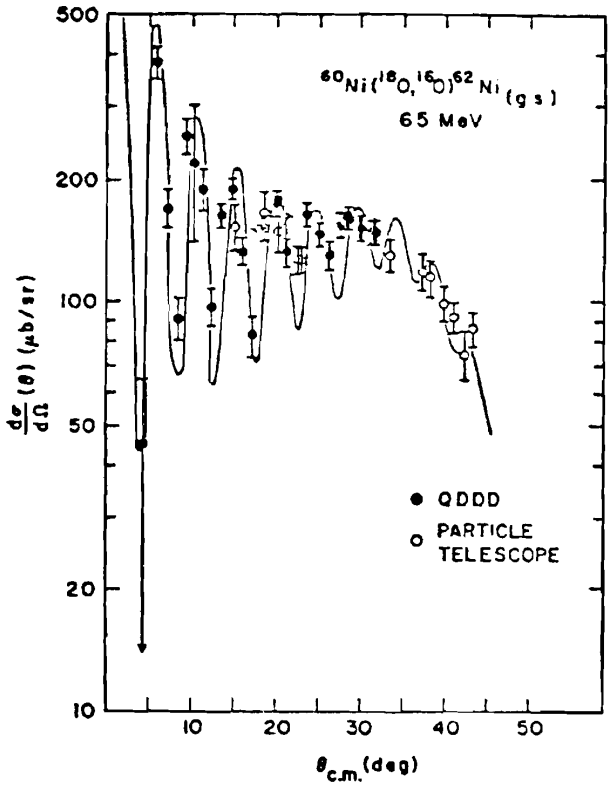

FIG. 8.7. Angular distribution corresponding to the $^{60}Ni(^{18}O, ^{16}O)$ transition to the ground state of ^{62}Ni measured at an incident laboratory energy of 65 MeV compared with a DWA theoretical prediction. [From LeVine, Baltz, et al. (74).]

where n is the effective index of refraction

$$n = \sqrt{1 - \frac{V}{E}}$$

By this means it is possible to construct a final wavefront, which, of course, will no longer be a plane wave.

The crucial point in the analysis of the small-angle $^{16}O + ^{58}Ni$ scattering is that different rays, 1 and 3 in Fig. 8.8, have the same angle of scattering. The amplitude at infinity is obtained by adding the *amplitude* of each of these two contributions. The rapid oscillations reflect the fact that as the angle of scattering changes, the net value of the amplitude will fluctuate as the relative phase of the two contributions changes. Constructive interference will give rise to the peaks and destructive interference to the valleys. For these oscillations to be observable, the magnitude of the contributing amplitudes must be comparable.

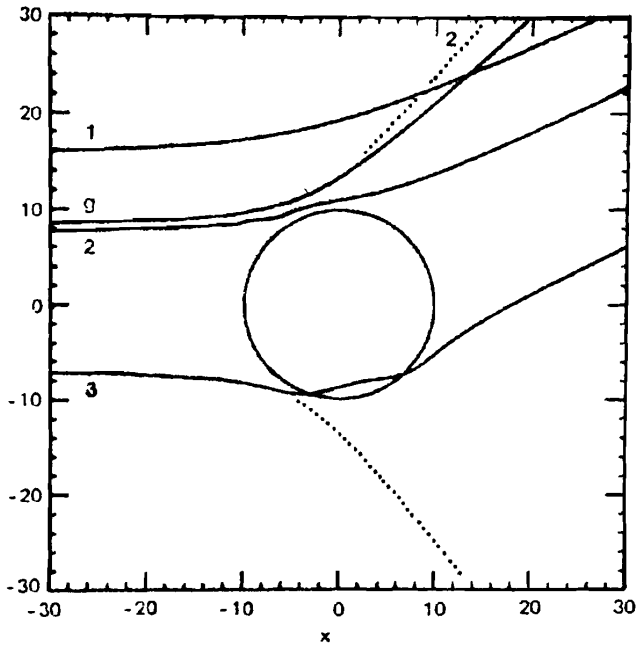

FIG. 8.8. Four classical orbits are plotted, three of which (1,2,3) scatter to the same angle. The grazing orbit is g. The circle marks the half-value of the Woods–Saxon nuclear potential. The orbits are for 100 MeV lab energy ^{18}O scattered by ^{120}Sn. Dotted lines show pure Coulomb orbits. The scale is in Fermi's [From Glendenning (75).]

This is possible only if the absorption in the surface region is not large, the conclusion noted earlier in this discussion.

9. REACTIONS WITH "EXOTIC" PROJECTILES

We have commented earlier on the reactions that can be induced by the exotic projectiles (π, K, $\bar{p}$, etc.). Their theoretical description does bring in some unique features that need to be addressed. For example, a pion interacting with a nucleon can form a Δ, the excited state of the nucleon. Therefore, an important intermediate state—a doorway state—which is formed in a pion–nucleus collision, is a Δ–hole state. The properties of the Δ–hole state are critically important for an understanding of pion-induced reactions and pion production. In pion production a Δ is formed in the collision of a nucleus with the incident projectile. The Δ then decays into a nucleon plus a pion. Because the Δ–hole state is generally a coherent combination of states with differing orbits for the Δ and for the hole, a single-step DWA direct reaction description will not suffice. Note that the π^+ couples strongly to the proton and weakly to the neutron in forming the Δ. The reverse is exhibited by the π^-, so that

pion–nucleon interaction is sensitive to the neutron and proton distributions. The double charge exchange reaction (see p. 16) requires the intervention of at least two nucleons and therefore is sensitive to the nucleon–nucleon correlations inside the nucleus.

When a kaon is incident on the target nucleus, it becomes possible to produce a Λ via the elementary reaction.

$$K^- + n \rightarrow \Lambda + \pi^- \tag{9.1}$$

If the Λ is captured by the nucleus, a hypernucleus will be formed. Capturing the Λ in a well-defined state is most likely if the nucleus does not fragment. Fragmentation can occur if the recoil momentum of the nucleon in the nucleus exceeds the Fermi momentum, which is on the order of 250 MeV/c for all but the lightest nuclei. [However, see Dalitz and Gal (76), who give a more stringent condition.]

A zero-momentum transfer is possible for the (K^-, π^-) reaction, for example [Podgoretsky (63); Feshbach and Kerman (66)]. In the elementary reaction equation (9.1), consider the case in which the neutron is at rest and the pion is observed in the forward direction. We shall now show that there is an incident kaon momentum for which the Λ produced is at rest. Under these circumstances conservation of energy and momentum (the momentum p of the kaon and the momentum of the pion are equal) requires

$$\sqrt{c^2p^2 + m_K^2c^4} + m_Nc^2 = m_\Lambda c^2 + \sqrt{c^2p^2 + m_\pi^2c^4}$$

It is a simple matter to solve this equation for the kinetic energy of the incident kaon:

$$E_K - m_Kc^2 = \frac{(m_K + m_N - m_\Lambda - m_\pi)(m_K + m_N - m_\Lambda + m_\pi)c^2}{2(m_\Lambda - m_N)}$$

Inserting the value of the masses yields a kinetic energy of about 231 MeV and a momentum of 531 MeV/c. At this energy the Λ produced will be at rest. In Table 9.1, the recoil Λ momenta, p_Λ, is given for a range of incident kaon momenta. Note that p_Λ equals the momentum transfer. Moreover, for a given kaon momentum, departure from the forward direction for the π^- increases the momentum transfer.

TABLE 9.1

p_K(MeV/c)	0	400	531	700	1000	2000
p_Λ(MeV/c)	250	40	0	40	75	130

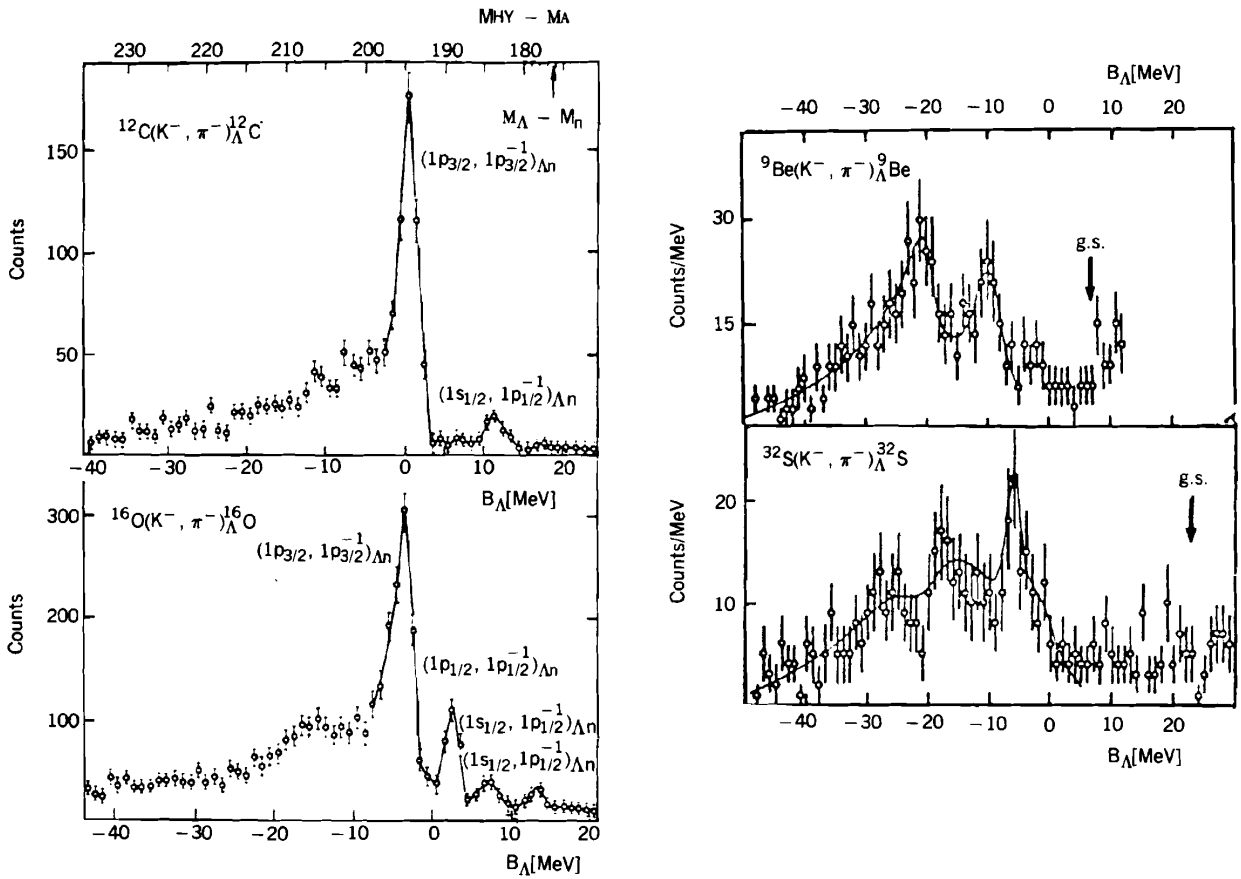

FIG. 9.1. Pion spectra obtained from the (K^-, π^-) reaction on ^{12}C, ^9Be, ^{16}O, and ^{32}S plotted as a function of the Λ binding energy, B_Λ. [From Brückner, Granz, et al. (76, 78).]

These results suggest that if a K^- in the momentum range sufficiently close to 531 MeV/c strikes a nucleus, it will be possible for the kaon to "strangeness exchange" with a nucleon, with the emergent pion going off in the forward direction, the Λ remaining behind and forming a hypernucleus in a definite state. One would expect a large cross section in this kaon momentum range, with the cross section being small elsewhere. This effect has been observed in a number of nuclei. In Fig. 9.1 we show the results obtained for $^{12}C(K^-,\pi^-)^{12}_{\Lambda}C$ and $^{16}O(K^-,\pi^-)^{16}_{\Lambda}O$ (at $p_K = 715$ MeV), where the pions are observed in the forward direction [Brückner, Granz, et al. (76, 78)]. A strong peak with a sizable cross section is clearly seen, confirming the existence of a direct strangeness exchange process.

The peaks are labeled by the orbit occupied by the Λ and the resulting neutron–hole. The major peaks are substitutional. The $p_{3/2}$ peak in ^{16}O consists of a Λ in a $p_{3/2}$ orbit about the host nucleus ^{15}O in a $p_{3/2}$ state, while in the $p_{1/2}$ case the ^{15}O is in a $p_{1/2}$ state. The splitting in ^{15}O between these two states is 6 MeV, with a maximum amount of 0.3 MeV which can be ascribed to the Λ spin–orbit interaction. It is therefore very small. The DWA calculation of Boussy (77) confirms this result. The Λ-nucleus spin-orbit potential is thus very much smaller than in the nucleon–nucleus case. Later experiments in which γ-ray transitions between hypernuclear energy levels were observed in a $(K^-,\pi^-\gamma)$ coincidence measurement. [May et al. (81)] confirmed this result.

We also note that an $(s_{1/2})_\Lambda(p^{-1}_{3/2})_n$ state is found. This illustrates an important point. In a hypernucleus, the Λ with a mass (1115.6 MeV) similar to the nucleon and indeed a member of the SU(3) octet $(n, p, \Lambda, \Sigma^\pm, \Sigma^0, \Xi^-, \Xi^0)$ does not need to satisfy the Pauli exclusion principle with respect to the nucleons in the nucleus. It can enter regions of configuration and momentum space forbidden to the nucleons. For example, the state $(s_{1/2})_n(p^{-1}_{3/2})_n$ is forbidden by the exclusion principle, but a Λ in the $s_{1/2}$ orbital about the ^{15}O host is allowed. From the point of view of the study of nuclear structure, the Λ in a hypernucleus acts as a baryonic probe, thereby providing another and quite different way to study nuclear properties.

10. SPECIFICITY AND SYMMETRY

The isolation of a given mode of interaction, which is one of the essential elements helping to ensure specificity, is greatly aided by symmetry requirements. These lead to selection rules that must be satisfied by the reaction. On the other hand, by studying the appropriate nuclear reactions and observing the selection rules, one can help determine the symmetries of the underlying elementary particle interactions and the accuracy with which they are satisfied. The discovery of parity nonconservation is a notable example of the use of nuclear properties for this purpose.

There are two kinds of symmetry of interest, intrinsic and space–time. The first is exemplified by charge, isospin, and strangeness. The second leads to such

overall conservation principles as conservation of linear and angular momentum, parity, and energy. Dynamically, the space–time properties of the fields that interact with nuclei are of fundamental importance. Since the vector potential $(\mathbf{A}, \phi)$ transforms as a 4-vector, the electromagnetic field couples with the 4-vector nuclear charge current $(\mathbf{J}, \rho)$ and thus serves as a probe of these nuclear properties. This coupling is required by Lorentz invariance of the Lagrangian, giving the interaction term $\mathbf{j}\cdot\mathbf{A} - \rho\phi$. The selection rules for electromagnetic transitions given in Chapter VIII of deShalit and Feshbach (74) are direct consequences of the transformation properties of $\mathbf{A}$ and ϕ. On the other hand, if the selection rules are known, it becomes possible to deduce these transformation properties.

In actual practice the transformation properties of the electromagnetic fields are used to identify the spins and parities of the levels of a nucleus by observing transitions induced by γ-rays, by the Coulomb field of heavy ions, or by the inelastic scattering of electrons.

Once these quantum numbers are established by, for example, observation of electromagnetic transitions, it becomes possible, by observing the transitions induced by another field, to determine its transformation properties. For example, nuclei can be used as "filters" that distinguish among the various symmetries of the weak interactions [Chapter IX of deShalit and Feshbach (74)]. In β-decay, by choosing the appropriate decaying nucleus and the appropriate final state, one can examine separately the Fermi and Gamow–Teller interactions. The superallowed $O^+ \rightarrow O^+$ transitions of isospin $T = 1$ nuclei [see deShalit and Feshbach (74, p. 788)] involve only the Fermi matrix element, $\langle \psi_f | \tau^{\pm} e^{i\mathbf{q}\cdot\mathbf{r}} | \psi_i \rangle$, while the decay of ^{6}He into ^{6}Li, from a spin O state to a spin 1, involves only the Gamow–Teller interaction, $\langle \psi_f | \tau^{\pm} \boldsymbol{\sigma} e^{i\mathbf{q}\cdot\mathbf{r}} | \psi_i \rangle$.

It is possible using neutrino-induced reactions [e.g., (ν, e^-)] and appropriate initial and final nuclear states, to select out various components of the weak interaction and obtain their momentum dependence. The results for the Fermi and Gamow–Teller matrix elements obtained from β-decay mentioned above involve only low momenta (i.e., small q) values. The selection rules for the neutrino-induced process are given in Table IX.17.2, of deShalit and Feshbach (74). By choosing appropriate initial and final states in the reaction, one can select out various combinations of terms in the Hamiltonian equation (IX.17.15).

Pion reactions can be used to explore the nature of the transition axial vector currents. For example, in a (γ, π) or (π, γ) reaction, the coupling to the nucleons must involve transition axial nuclear currents because of the pseudoscalar nature of the pion. The leading term of the (γ, π) reaction amplitude near threshold is proportional to

$$\left\langle \psi_f \left| \sum_i \tau^{\pm} \boldsymbol{\sigma}_i \cdot \mathbf{E} \phi \right| \psi_i \right\rangle$$

where $\mathbf{E}$ is the electric field associated with the γ-ray and ϕ is the pion field wave function. We see that the Gamow–Teller combination is involved, while

the axial current is given by $\sum_i \tau_i^{\pm} \boldsymbol{\sigma}_i$. The connection of the pion transition to the weak interaction is not in retrospect surprising because of the relation between the axial current and the pion field given by PCAC [see (IX.14.4) of deShalit and Feshbach (74)]. Similarly, the (K,π) reactions can probe the transition and exchange strangeness currents.

Intrinsic symmetries will also provide selection rules that select reaction modes. Strictly speaking, isospin is not conserved in nuclear reactions because the Coulomb interaction violates isospin conservation. However, the effects of Coulomb force, such as the Coulomb barrier on either the incident channel or on the exit channel or both, can be taken into account. One may then ask: Upon making this correction, will the remaining features of the reaction conserve isospin? In other words, is the effect of the Coulomb field (or other isospin breaking interactions) of importance only when the projectile approaches the target or when the emergent particle leaves the residual nucleus? The answer appears to be that isospin is usually conserved in one-step direct reactions once the external effects of the Coulomb field are taken into account. However, the question of whether isospin is conserved in multistep processes is more difficult to answer in general. One would expect it to hold if there are only a few steps involved but that as the number of steps increases it would begin to fail. The expectation that isospin is conserved in direct processes relies on the long range of the Coulomb potential, which as a consequence has small nondiagonal matrix elements connecting states of differing isospin. The Coulomb potential can have substantial diagonal elements, giving rise to substantial energy shifts (the *Coulomb energy*). An excellent example of this effect is seen in the isobar analog state, which differs substantially in energy from its parent state because of the Coulomb interaction but whose wave function is hardly affected because its nondiagonal matrix elements between states of differing isospin are small [see the discussion on p. 102 of deShalit and Feshbach (74)]. However, in the multistep processes one has the possibility that the isospin (conservation) violation accumulates after a number of steps and become appreciable. It should also be borne in mind that the effect of the isospin violating interaction depends not only on the magnitude of the nondiagonal matrix element but also on the density of final states; the greater their number at the right energy, the greater the probability of a transition. The relevant additional fact is that the density of levels goes up very rapidly with the number of steps. It thus seems likely that if a reaction involves more than a few steps, isospin is probably not conserved. We would, for example, not expect isospin conservation in the evaporation part of the spectrum. This is indeed observed.

A rather striking example of the breakdown of isospin conservation occurs in the (α,γ) process. The α-particle has zero isospin, while the γ-ray can be considered for the energy domain under investigation to have unit isospin. The process therefore involves a change $\Delta T = 1$ between the initial and final nuclei. Under these circumstances, the process $^{28}\mathrm{Si}(\alpha,\gamma_0)^{32}\mathrm{S}$ leading to the ground state of $^{32}\mathrm{S}$ is isospin forbidden, whereas $^{30}\mathrm{Si}(\alpha,\gamma_0)^{34}\mathrm{S}$ is allowed. But, in fact, the cross section for the first of these is larger than the cross section for

the second! The explanation seems to be that a number of steps must be involved as the system proceeds from the capture of the α-particle to the final release of the γ-ray.

Isospin symmetry is broken because of the interaction carried by the electromagnetic field. That interaction can be considered to be transmitted by the interchange of the photon by the interacting systems. When we extend our considerations to include the strange particles, isospin symmetry is extended to the SU(3) symmetry. If isospin symmetry were exact, the masses of the neutron and proton would be identical. If SU(3) symmetry were exact, the masses of the neutron, proton, Λ, $\Sigma^{(+,0,-)}$, and $\Xi^{(-,0)}$ would be identical. They are not. The Λ–proton mass difference, for example, is 177.3 MeV. This symmetry breaking (in addition to the electromagnetic variety described above) is thought to be a consequence of the mass of the strange quark, which differs from that of the up and down quarks. Recall that the proton consists of two up quarks and one down quark, while the Λ is made up of an up, a down, and a strange quark. Symmetry breaking of the baryon–baryon forces occurs because the kaons and pions are massive; the forces they transmit have a finite range given by their Compton wavelength, which is on the order of 0.4 and 1.4 fm, respectively. It is clear that in contrast with the Coulomb potential, the differences between the nuclear matrix elements of the forces generated by pion and kaon exchange will not be small and thus SU(3) symmetry is broken. However, it is possible, as in the Coulomb case, that the nondiagonal matrix elements between states specified by SU(3) quantum numbers are small. In that event, SU(3) analog states would exist.

We conclude this section with two examples of the impact of symmetry on nuclear reactions. Spatial symmetries in the angular distribution of reaction products can be a consequence of the statistics satisfied when the projectile and target are *identical*. The simplest case is provided by the elastic scattering of a ^{12}C nucleus by another ^{12}C nucleus. This system obeys Bose statistics; that is, the wave function of the system must be symmetric with respect to the exchange of the two ^{12}C nuclei. The wave function for the system can be written as follows:

$$\phi(\xi_a)\phi(\xi_b)\chi(\mathbf{R}_a - \mathbf{R}_b)$$

where $\phi(\xi_a)$ is the wave function describing the ^{12}C particle and ξ_a represents all the internal coordinates. The wave function χ describes the relative motion of the two nuclei, depending only on the center of mass $\mathbf{R}_a$ and $\mathbf{R}_b$ of each of the particles. From the Bose symmetry it follows that

$$\chi(\mathbf{R}_a - \mathbf{R}_b) = \chi(\mathbf{R}_b - \mathbf{R}_a)$$

Hence asymptotically,

$$\chi(\mathbf{R}_a - \mathbf{R}_b) \to \frac{1}{\sqrt{2}}[e^{ik\cdot(\mathbf{R}_a - \mathbf{R}_b)} + e^{-ik\cdot(\mathbf{R}_a - \mathbf{R}_b)}] + [f(\theta) + f(\pi - \theta)]\frac{e^{ik|\mathbf{R}_a - \mathbf{R}_b|}}{|\mathbf{R}_a - \mathbf{R}_b|} \tag{10.1}$$

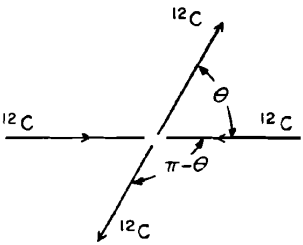

FIG. 10.1

where

$$\cos\theta = \frac{\mathbf{k}\cdot(\mathbf{R}_a - \mathbf{R}_b)}{k|\mathbf{R}_a - \mathbf{R}_b|}$$

The scattering amplitude

$$f(\theta) + f(\pi - \theta) \tag{10.2}$$

is symmetric about 90°, which simply reflects the identity of the two ^{12}C nuclei, as can be seen in Fig. 10.1. It is not possible to determine which of the two ^{12}C nuclei scattered through the angle θ and which through the angle $(\pi - \theta)$. The plus sign between the two amplitudes is a consequence of the Bose statistics obeyed by the ^{12}C nuclei. Fermi statistics implies the opposite sign.

More generally, Bose statistics imply that the only even-parity wave functions enter into the incident wave [see the first two terms in (10.1), which describe the incident wave for a two-body Bose system], and therefore (assuming conservation of parity) *only even-parity wave functions are to be found in the emerging wave.* This conclusion applies not only to elastic scattering but also to reactions. Thus in the ^{12}C(^{12}C, α)^{20}Ne reaction, as a consequence of the Bose statistics of ^{12}C, only even-parity states of the $\alpha + {}^{20}$Ne system are generated.

These arguments are readily generalized to particles with spin. Nuclei with an old number of nucleons obey Fermi statistics, while even-A nuclei obey Bose statistics. A simple example is the scattering of identical spin-$\frac{1}{2}$ particles, such as protons or ^{17}O nuclei. One can classify the spin states of the system as singlet and triplet, the first of which is odd under exchange, the second even. To satisfy the requirements of Fermi statistics, the spatial wave function for the singlet state should be even under exchange, whereas for the triplet state the spatial wave function is odd. The former then has even parity, the latter odd parity, so that for the triplet state the scattering amplitude has the form

$$f(\theta) - f(\pi - \theta)$$

and is zero at $\theta = \pi/2$.

A general theorem derived, for example, by C. N. Yang deals with the maximum complexity to be expected in an angular distribution. Consider, for simplicity, the collision of a spinless system by a spinless, target leading to

spinless products. The maximum angular momentum L_i brought in by the incident wave that will make significant contributions to the collision is determined by the Coulomb and angular momentum barriers. The limit imposed by the latter is approximately

$$L_i \sim k_i R$$

where k_i is the incident wave number and R is the radius determined by the range of the interaction. Similarly, there will be a limit to angular momentum of the final system given by L_f. The theorem states that when the angular distribution is decomposed into Legendre polynomials P_L, the maximum value of L will be the minimum of the two values $2L_i$ and $2L_f$. The theorem can readily be understood on the basis of the information content of both the

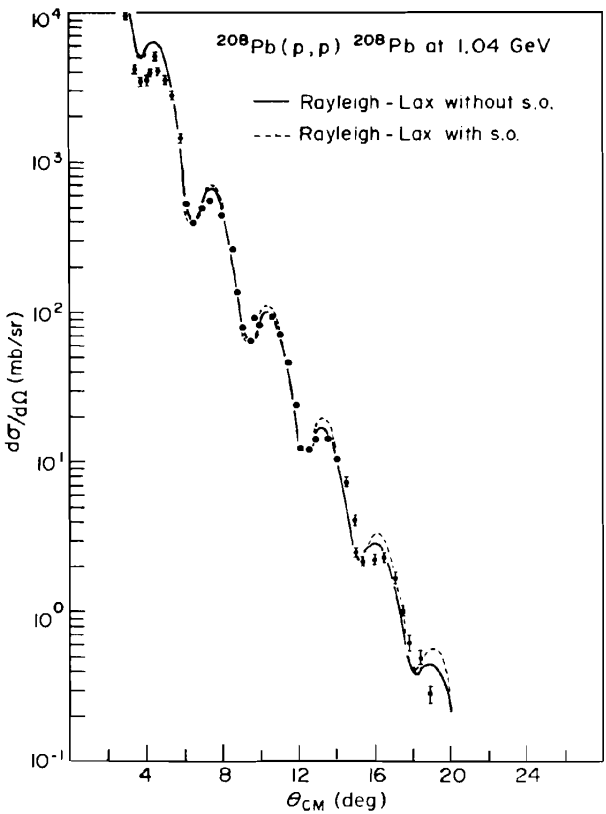

FIG. 10.2. Comparison of experimental angular distribution for the elastic scattering of 1.04-GeV protons by ^{208}Pb with the predictions employing the Rayleigh–Lax potential with and without spin-orbit (s.o.) terms. The density-dependent Hartree–Fock densities are used. [From Boridy and Feshbach (77).]

incident and emerging waves. For example, if the highest-order Legendre polynomial entering in the incident wave is P_{L_i}, the incident direction is defined with an uncertainty of $O(1/L_i)$. The collision process cannot reduce this uncertainty, so that the maximum order of the Legendre polynomials in the emerging amplitude certainly cannot exceed L_i. The angular distribution involves the square of the amplitude and thus the limit of $2L_i$ is obtained. When spin is introduced the theorem now states that the maximum value of L is the minimum of $2L_i$, $2L_f$, and $2J$, where J is the maximum value of the total angular momentum of the system entering in the reaction. A simple consequence of this discussion is that the angular distribution for the elastic scattering will exhibit oscillations whose period is greater than or on the order of $1/kR$. At very high energies or for strongly absorbed particles the oscillations are of the order of $(1/kR)$ (see Fig. 10.2).

Problem. Prove that the only states of a spin-zero nucleus that can be excited by the forward ($\theta = 0$) inelastic scattering of α-particles are the natural parity states, 0^+, 1^-, 2^+,..., $J^{(-1)^J}$,.....

11. DENSITIES, CORRELATIONS, AND THE DIRECT REACTIONS

In the preceding sections and in Sections I.12 to I.15 of deShalit and Feshbach (74), we have reviewed some of the elementary concepts that are useful for the understanding of nuclear reactions. We have seen how by choosing the appropriate experimental parameters—target, projectile and its energy, type of reaction, excitation energy of residual nucleus, energy resolution, and angular definition that can be obtained with the detection apparatus—one can select the type of final state excited and determine its properties. These detailed studies for a wide range of experimental parameters are essential for a deep and broad understanding of the properties of nuclei. In this final section we discuss the long-range goals of nuclear reaction studies, which go beyond the discovery of the "simple" degrees of freedom, the nuclear normal modes of motion.

A principal goal is the determination of the nuclear Hamiltonian, that is, the detailed description of the forces that determine nuclear structure and the interaction of nuclei with a variety of particles, and the form to which these reduce for the nuclear normal modes. The energy spectrum of a nucleus is very useful in this respect. The Hamiltonian of Chapter VI in deShalit and Feshbach (74), for example for rotational deformed nuclei, was in the long run mostly, but not entirely, justified by the observed rotational energy spectrum. But, in addition, properties of the nuclear wave function such as the B coefficients for radiative transition probabilities provided important supporting evidence. If we wish to go beyond the model Hamiltonian, much more information on the nuclear wave function is required; in fact, if we knew the nuclear wave function for one state with "infinite" accuracy, it would be possible to determine the nuclear Hamiltonian.

Interestingly, the one-step direct reactions provide the most direct information on the nuclear wave function. Perhaps the most outstanding example is the use of elastic and inelastic electron scattering to determine the charge and current density inside nuclei.

Formally, the amplitude for a transition of a target nucleus with wave function Ψ_T to the residual nucleus with wave function Ψ_R can always be cast into the form

$$\mathcal{T}_{RT} = \langle \Psi_R | \hat{\mathcal{T}} \Psi_T \rangle \tag{11.1}$$

The operator $\hat{\mathcal{T}}$ depends on the coordinates of the problem, including positions, momenta, spins, and isospins, and on the state of the incident projectile and the emergent particle. As is apparent from the form of (11.1), the observation of the transition will yield information on the overlap Ψ_T with Ψ_R, its nature depending on whether $\hat{\mathcal{T}}$ is a one-body, a two-body, or a more general, many-body operator. When the residual and target nucleus have the same mass number, that is, when scattering occurs, for example, in the (p,p) or (p,p') reaction, and when $\hat{\mathcal{T}}$ is a one-body operator‡ as regards its dependence on target nucleons,

$$\hat{\mathcal{T}} = \sum_i \hat{\mathcal{T}}(i) \tag{11.2}$$

(presuming symmetry), Equation (11.1) becomes

$$\hat{\mathcal{T}}_{RT} = \sum_i \int \Psi_R^*(1,2,\ldots,A)\hat{\mathcal{T}}(i)\Psi_T(1,2,\ldots,A)d(1)\cdots$$

where the integration refers to summation over spin and isospin and integration over spatial coordinates. The center-of-mass motion of the residual and target nuclei will be included in the operator $\hat{\mathcal{T}}$ so that Ψ_R and Ψ_T depend only upon internal coordinates. The spatial integrations are then over $3(A-1)$ coordinates. The remaining three coordinates are those of the center of mass. Using the symmetry of $\hat{\mathcal{T}}$ and the wave functions, one finds that

$$\mathcal{T}_{RT} = A \int \Psi_R^*(1,\ldots,A)\hat{\mathcal{T}}(1)\Psi_T(1,\ldots,A)d(1)\cdots$$

or

$$\mathcal{T}_{RT} = A \int \rho_{RT}^{(1)}\hat{\mathcal{T}}(1)d(1) \tag{11.3}$$

‡More generally $\hat{\mathcal{T}} = \sum_{i,i'} \hat{\mathcal{T}}(i|i')$. This form leads to more complicated results which we discuss later [see (11.10)].

where $\rho_{RT}^{(1)}$ is the density matrix:

$$\rho_{RT}^{(1)} = \int \Psi_R^*(1,2,\ldots,A)\Psi_T(1,2,\ldots,A)d(2)\cdots \tag{11.4}$$

The experiment can provide the values of $\mathscr{T}_{RT}$ (more precisely $|\mathscr{T}_{RT}|^2$) as a function of energy, momentum transfer, and finally, energy transfer if the scattering is inelastic. From that one hopes to deduce $\rho_{RT}^{(1)}$ or at least to compare with $\mathscr{T}_{RT}$ computed using a $\rho_{RT}^{(1)}$ based on theory and/or other experiments. Elastic electron scattering can be used to determine the charge density of a number of nuclei. The density refers to the diagonal value of $\rho_{RT}^{(1)}$, $\rho_{TT}^{(1)}$. Similarly, inelastic electron scattering can be used to determine nondiagonal elements of $\rho_{RT}^{(1)}$.

Problem. Prove that when $\hat{\mathscr{T}} = \sum_{i,i'} \hat{\mathscr{T}}(i'|i)$, $\mathscr{T}_{RT} = A \operatorname{tr} \rho_{RT}(i|i')\hat{\mathscr{T}}(i|i')$, where the trace is carried out with respect to spin, isospin, and spatial coordinates.

Obviously, the question arises of when the operator $\hat{\mathscr{T}}$ is a one-body operator. It clearly has that character when the underlying interaction between the projectile and target is weak or electromagnetic in character, for then first-order perturbation theory may be applied. It also has that character for *single-step* direct reactions. Generally, $\hat{\mathscr{T}}$ for a multistep direct or compound nuclear reaction is a many-body operator.

There are several types of densities: matter density, charge density, spin density, and spin–isospin density. The latter describes the probability per unit volume of finding a particular particle (i.e., neutron or proton) with a particular spin orientation at a point within the nucleus. Equation (11.4) for $\rho_{TT}^{(1)}$ is just the matter density. It is convenient to rewrite it and ρ_{RT} as the matrix element of the operator $\hat{\rho}(\mathbf{r})$:

$$\hat{\rho}(\mathbf{r}) = \frac{1}{A}\sum \delta(\mathbf{r} - \mathbf{r}_i) \tag{11.5}$$

where $\mathbf{r}_i$ is the coordinate of a nucleon and

$$\rho_{RT}^{(1)}(\mathbf{r}) = \langle \Psi_R | \hat{\rho} \Psi_T \rangle \tag{11.6}$$

The expression for the charge density $\hat{\rho}^{(c)}$ is

$$\hat{\rho}^{(c)}(\mathbf{r}) = \frac{1}{A}\sum_i \tfrac{1}{2}[1 + \tau_3(i)]\delta(\mathbf{r} - \mathbf{r}_i) \tag{11.7}$$

while the spin and spin–isospin density operators are

$$\hat{\rho}_\alpha^{(\sigma)}(\mathbf{r}) = \frac{1}{A}\sum_i \sigma_\alpha(i)\delta(\mathbf{r} - \mathbf{r}_i) \tag{11.8}$$

$$\rho_{\alpha\beta}^{(\sigma\tau)}(\mathbf{r}) = \frac{1}{A}\sum_i \sigma_\alpha(i)\tau_\beta(i)\delta(\mathbf{r}-\mathbf{r}_i) \tag{11.9}$$

The diagonal ground-state values of $\hat{\rho}^{(c)}$ are quite well known. Its nondiagonal values and the matrix elements of $\hat{\rho}^{(\sigma)}$ are now in the process of being determined by elastic and inelastic electron scattering. Further information is also provided by the scattering of high-energy protons and pions by nuclei.

Equation (11.2) provides an accurate representation of one-body operators only if the interaction between the projectile and the target nucleon is sufficiently weak. For the strong interactions, (11.2) is replaced by

$$\hat{\mathscr{T}} = \sum_{i',i} \hat{\mathscr{T}}(i'|i) \tag{11.10}$$

and $\hat{\rho}_{RT}$ now becomes a matrix not only with respect to the subscripts R and T but also with regard to space [see (III.4.4) in deShalit and Feshbach (74)]:

$$\rho_{RT}(i|i') = \int \Psi_R^*(i,2,\ldots)\Psi_T(i',2,\ldots)d(2)\cdots \tag{11.11}$$

The spatial matrix properties of this full $\rho_{RT}(i'|i)$ can be exploited to obtain nuclear information of even greater subtlety than, say, that obtained from $\hat{\rho}^{(c)}$. For example, take the diagonal

$$\rho(i'|i) \equiv \rho_{TT}(i'|i) \tag{11.12}$$

It can be considered as a Hermitian matrix in i' and i, and as a consequence, can be diagonalized. The procedure will be described later (see p. 203). For the moment it is sufficient to state the result:

$$\rho(i'|i) = \sum_\lambda \psi_\lambda^*(i')\psi_\lambda(i)\kappa_\lambda \tag{11.13}$$

The functions $\psi_\lambda(i)$ are orthogonal and can be normalized. They are the best single-particle wave functions for the description of the target, at least as for as the reactions leading to the determination of $\rho(i'|i)$ are concerned.

One-particle transfer reactions such as (p,d) or $(p,2p)$ are frequently used to determine the properties of single-particle wave functions. The analog of ρ_{RT} for this case is

$$S_{RT}(1) = \int \Psi_R^*(2,3,\ldots,A)\Psi_T(1,2,\ldots,A)d(2)\cdots \tag{11.14}$$

Clearly, if Ψ_T differed from Ψ_R by the addition of one orbital to a Slater determinant, $S_{RT}(1)$ would be proportional to the corresponding single-particle

wave function. The square magnitude of the constant of proportionality gives the probability that Ψ_T consists of Ψ_R and a particle in a particular single-particle state and is known as the spectroscopic factor. If Ψ_R is a complex combination of excitations, this constant will be small, and in the absence of other effects originating in $\hat{\mathscr{T}}$, the cross section will be reduced. The cross section for one-particle transfer reactions tends to be largest when the shell model description is most applicable.

Returning to scattering, two-particle density matrices [see (III, 4.9) in deShalit and Feshbach (74)] appear when the operator $\hat{\mathscr{T}}$ is a two-body operator:

$$\hat{\mathscr{T}} = \sum_{i<j} \hat{\mathscr{T}}(i,j) \tag{11.15}$$

The resultant $\mathscr{T}_{RT}$ is then

$$\mathscr{T}_{RT} = \tfrac{1}{2}A(A-1)\int \Psi_R^*(1,2,\ldots,A)\hat{\mathscr{T}}(1,2)\Psi_T(1,2,\ldots,A)d(1)\cdots$$

or

$$\mathscr{T}_{RT} = \tfrac{1}{2}A(A-1)\int \rho_{RT}^{(2)}(1,2)\hat{\mathscr{T}}(1,2)d(1)d(2)$$

where

$$\rho_{RT}^{(2)}(1,2) = \int \Psi_R^*(1,2,3,\ldots,A)\Psi_T(1,2,3,\ldots,A)d(3)\cdots \tag{11.16}$$

The corresponding operator is

$$\hat{\rho}^{(2)}(\mathbf{x},\mathbf{y}) = \frac{2}{A(A-1)}\sum_{i<j}\delta(\mathbf{x}-\mathbf{r}_i)\delta(\mathbf{y}-\mathbf{r}_j) \tag{11.17}$$

The pair correlation function $C^{(2)}(x,y)$ is defined by

$$C^{(2)}(\mathbf{x},\mathbf{y}) = \hat{\rho}^{(2)}(\mathbf{x},\mathbf{y}) - \hat{\rho}(\mathbf{x})\hat{\rho}(\mathbf{y}) \tag{11.18}$$

It has the property

$$\int C^{(2)}(\mathbf{x},\mathbf{y})\,d\mathbf{x} = \int C^{(2)}(\mathbf{x},\mathbf{y})\,d\mathbf{y} = 0 \tag{11.19}$$

since

$$\int \hat{\rho}^{(2)}(1,2)d(1) = \hat{\rho}^{(1)}(2)$$

Pair correlations for both elastic and inelastic scattering will be present whenever the interactions are sufficiently strong. They therefore can play an important role for hadron interactions with nuclei. Some information on the diagonal

ground-state two-body density is available from the calculation of the binding energy of nuclei [see (III.4.11) in deShalit and Feshbach (74)].

Spin and isospin components of the correlation function can be obtained through the use of appropriate operators. The operator

$$\hat{\rho}^{(2)}_{s=0} = \frac{2}{A(A-1)} \sum_{i<j} \delta(\mathbf{x} - \mathbf{r}_i)\delta(\mathbf{y} - \mathbf{r}_j)\tfrac{1}{4}(1 - \boldsymbol{\sigma}_i \cdot \boldsymbol{\sigma}_j) \tag{11.20}$$

gives the probability density of finding a pair of nucleons at $\mathbf{x}$ and $\mathbf{y}$ in the singlet ($S = 0$) state. Similarly,

$$\hat{\rho}^{(2)}_{S=1,T=0} = \frac{2}{A(A-1)} \sum_{i<j} \delta(\mathbf{x} - \mathbf{r}_i)\delta(\mathbf{y} - \mathbf{r}_j)\tfrac{1}{4}(3 + \boldsymbol{\sigma}_i \cdot \boldsymbol{\sigma}_j)\tfrac{1}{4}(1 - \boldsymbol{\tau}_i \cdot \boldsymbol{\tau}_j) \tag{11.21}$$

gives the probability density of finding a pair of nucleons at $\mathbf{x}$ and $\mathbf{y}$ in the spin triplet ($S = 1$) and isospin singlet ($T = 0$) state. These will appear in $\mathcal{T}_{RT}$ if the two-body operator $\hat{\mathcal{T}}(1,2)$ has a spin and isospin structure which necessarily will appear in the form exemplified by (11.20) and (11.21).

Two-body transfer reactions [e.g., $(p, {}^3\mathrm{H})$] will provide information on the two-body wave functions since it will involve overlap integrals of the form

$$S^{(2)}_{RT}(1,2) = \int \Psi^*_R(3,4,\ldots,A)\Psi_T(1,2,3,4,\ldots,A)d(3)\cdots \tag{11.22}$$

Deviations of $S^{(2)}_{RT}(1,2)$ from the product of single-particle wave functions, which might be obtained from single-particle transfer reactions (11.14), would reflect the presence of correlations in the wave function Ψ_T. In the case of the $(p, {}^3\mathrm{H})$ reaction, there is a pronounced sensitivity to correlations in which the two neutrons ($T = 0$) are in a ${}^1S_0$ state.

Generally, correlations may be needed to describe a process when the strong interactions are involved. Highly accurate studies with the weak and electromagnetic interactions could in principle provide information on the correlations—that is, if the accuracy required second-order perturbation theory in order to obtain a sufficiently precise prediction. For strong interactions, the multistep processes will generally be sensitive to correlations. This can most easily be seen in the high-energy limit, for which it is possible to picture the reaction as preceeding by a number of collisions between the nucleons in the target and the projectile. Clearly, if two such collisions are important, the consequences will depend on the pair correlations in the target; if three, the triple correlations will be relevant; and so on.

We can extend this discussion to include third- and higher-order density matrices and correlations. We have, however, already shown that a principal result of the study of reactions will be the determination of properties of the wave functions of the target and residual neclei. If it were possible to carry out

all the indicated evaluations (it is probably not necessary or desirable to carry out all of them), one would determine the nuclear wave function and thereby the nuclear Hamiltonian, which is the ultimate goal of the study of nuclear structure. We are a very long way indeed from carrying out this ambitious task, and the description given above is almost certainly overidealized. The outstanding example of the application of this analysis is the use of elastic and inelastic electron scattering to determine the charge and current density inside nuclei. More recently, high-energy proton scattering by nuclei has begun to achieve similar results for the matter density.

Problem. Define $\hat{\rho}^{(3)}(\mathbf{x}, \mathbf{y}, \mathbf{z})$. Show that the third-order correlation function is

$$C^{(3)}(\mathbf{x}, \mathbf{y}, \mathbf{z}) = \rho^{(3)}(\mathbf{x}, \mathbf{y}, \mathbf{z}) - \rho(\mathbf{x})\rho^{(2)}(\mathbf{y}, \mathbf{z}) - \rho(\mathbf{y})\rho^{(2)}(\mathbf{x}, \mathbf{z}) - \rho(\mathbf{z})\rho^{(2)}(\mathbf{x}, \mathbf{y}) + 2\rho(\mathbf{z})\rho(\mathbf{y})\rho(\mathbf{x})$$

Show that $\int C^{(3)}\, d\mathbf{x} = 0$.